Numerical Electromagnetic Field Analysis of Tower Surge Response by Moment Method

モーメント法による鉄塔サージ特性の数値電磁界解析

Yoshihiro BABA
67113

Supervised by Prof. Masaru ISHII

Department of Electrical Engineering
The University of Tokyo

December 18, 1998

論文の内容の要旨

論文題目

Numerical Electromagnetic Field Analysis of Tower Surge Response by Moment Method

（モーメント法による鉄塔サージ特性の数値電磁界解析）

馬場　吉弘

送電線の雷による事故について検討する場合，雷が送電線に落ちるか否かが重要である。送電線への落雷は鉄塔や架空地線への雷撃と，架空地線をかいくぐって電力線に直撃するいわゆる遮へい失敗に分類される。鉄塔あるいは架空地線に雷撃があると，雷電流は鉄塔を経由して大地に流入するが，この過程で，がいし連両端に過電圧が発生し，時には逆フラッシオーバに至る場合がある。送電線の雷事故は，この逆フラッシオーバに起因したものがほとんどであり，遮へい失敗によるものは僅かであることが知られている。送電線近傍の構造物や大地への落雷も送電線に過電圧を誘導するが，その電圧が送電線の絶縁を脅かすまでには至らない。このため，送電線や変電所の耐雷設計を行う上で，逆フラッシオーバ現象を厳密に解析・予測することが極めて重要である。

逆フラッシオーバ現象を支配する主要因の一つとして挙げられるのが，本論文で対象とする鉄塔のサージ特性である。特に，最近建設が進んでいる 100 万V 2回線送電線では鉄塔が高く，鉄塔内の進行波の往復伝搬時間が雷撃電流の立ち上がり時間に近くなるため，その特性ががいし連両端に生じる電圧に与える影響はますます大きくなる。このため，種々の手法により研究が続けられているが未だに広く合意が得られるには至っていない。

鉄塔のサージ特性は，回路モデル上ではそれを伝送線路で表現することが多いため，鉄塔サージインピーダンスという代表値で表現されることが多い。それを評価する方法として，実鉄塔における測定，縮小モデルによる測定，解析的手法による電磁界の計算がこれまで利用されてきた。実鉄塔における測定は，その規模の大きさのため理想的な配置で実験を行うのは極めて困難であ

る。縮小モデルによる測定は，理想的な配置で実験ができ，それにかかる人手や時間が大幅に短縮できるという利点があるが，測定対象に与える測定用機器の存在の影響が無視できないことから測定精度に難点がある。このため，これまでのところ得られた結果が実用的な目的に使用された実績はない。電磁界理論により解析的に鉄塔サージインピーダンスを導出しようという場合には，鉄塔を円錐や円筒のような単純な形状に近似する必要があり，問題の定性的な理解を助けるという意義はあるが，実用的な目的には向いていない。

本論文では，この問題にモーメント法に基づく三次元数値電磁界解析コード NEC-2 を適用することにより鉄塔サージ特性の検討を行った。本コードは 20 年程前に米国のローレンス・リバモア国立研究所で開発され，以来，線状アンテナの標準的な電磁界解析用ツールとして広く使用され続けている。本コードを採用したのは，鉄塔や送電線も線状導体から構成されているため，それらの特性を評価するのに最適であると判断したためである。

先ず，立体回路に誘導される電圧・電流の実験結果との比較により，NEC-2 の適用可能性を検討し，計算値と実験値との相違が 5 % 程度であることを実証した。この数値は実験で通常保証される精度と同等以上であり，極めて良好である。

この成果に基づき，NEC-2 を用いて鉄塔サージインピーダンスの測定法を模擬したシミュレーションを行い，測定法および補助線配置の測定結果に与える影響を調べた。その結果，標準的な形状の 2 回線鉄塔のサージインピーダンスは，がいし連両端に生じる電圧に着目する直接法により鉄塔単体を対象に評価した場合 150 Ω 程度となること，架空地線と鉄塔のインピーダンスの比に着目する透過波法で評価した場合にはそれより 10 % 程度低い値となることが明らかになった。

同様に，架空地線を有する鉄塔のサージ特性の直接法による評価を NEC-2 を用いて行った。その結果，立ち上がり時間が数 μs の雷電流が流入した場合でも，がいし連電圧がピーク値をとる時点では，鉄塔に分流する電流がつくる強力な上向き電界の影響で，架空地線 – 相導体間の結合率は定常値の 50 % 前後の大幅に低い値となるという新事実が明らかになった。また，現象自体は既に知られていたが，その原因が未だ明らかにされていない初期に高い鉄塔接地インピーダンスについて検討を行った。その結果，鉄塔を流れる急峻波電流自体が強力な軸方向電界をつくり電流波の波頭部を変歪させ，また鉄塔の根開きした脚部構造が非均質な導波路として作用するため球面波の反射を不完全なものにしているという 2 つの物理現象がその背景にあることが明らかになった。

最後に，架線された鉄塔における上述の複雑な物理現象を EMTP で再現するための等価回路モデルとそのパラメータについて検討を行い，良好な再現性を有するモデルとパラメータ選定手法を提案した。選定した回路モデル上での鉄塔頂部のサージインピーダンスは，初期に低い結合率を考慮したため，単体で評価した場合の 150 Ω に比べ 35 % も高い 200 Ω 程度になる。

以上の成果は，雷サージの評価手法について電気学会でまとめられた最新の技術報告にも取り入れられており，今後の雷サージ解析に反映され，解析精度の向上に寄与するものと思われる。

Abstract

In analyzing the lightning performance of overhead power transmission lines and substations, the lightning surge characteristics of transmission line components are important as well as the statistics of lightning parameters such as the ground flash density, the stroke peak current distributions and so on. Various studies, therefore, have been done to measure the surge characteristics of the line components and to develop their equivalent circuit models for the EMTP simulations. The tower surge characteristics including the footing impedance are among the most fundamental factors in the analysis since they contribute directly to the insulator voltages during a lightning hit. Particularly for such tall structures as EHV or UHV double-circuit towers, the characteristics become more dominant owing to the longer round-trip time of a traveling wave in the tower. An agreement on the interpretation of this phenomenon, however, has not been reached yet.

There have been three representative methods to evaluate the transient characteristics of a tower as follows: (i) measurements on full-sized towers, (ii) measurements on reduced-scale models and (iii) theoretical studies. Measurements on full-sized towers are straightforward in evaluating the actual characteristics of a tower struck by lightning, however, it is difficult to carry out this kind of experiments in the ideal arrangement where a current lead wire is stretched vertically above the tower top to simulate a lightning channel, owing to its scale. Measurements on reduced-scale models are more economical than those on full-sized towers, and are flexible in setting up various experimental arrangements. It is, however, not easy to maintain the accuracy of the measurement. Theoretical studies on simplified geometry may be useful in understanding the phenomenon, however, they are impotent for accurate evaluation of the dynamic electromagnetic behavior of a three-dimensional system struck by lightning.

For the accurate analysis of the dynamic electromagnetic field around a complex tower system struck by lightning, electromagnetic modeling codes are applicable. Among many available codes, the Numerical Electromagnetic Code (NEC-2) based on the Method of Moments is chosen for the present work, since it has been widely and successfully used in analyzing thin-wire antennas, and a tower system can be regarded as a thin-wire antenna.

In the present thesis, firstly, the applicability of NEC-2 to the electromagnetic field analysis

of tower surge response is verified by comparison with experimental results on simple structures. The difference is less than about 5 %, which is within the accuracy maintained in the measurements.

Secondly, the effects of the measuring methods and the arrangements of the measuring wires on the evaluated tower surge impedance are studied using NEC-2. On the basis of the analyses, the surge impedance of an independent double-circuit tower is estimated to be about 150 Ω when it is evaluated by the direct method, where a current lead wire simulating a lightning channel is stretched vertically and a voltage measuring wire is stretched horizontally. The tower surge impedance representing the current splitting ratio at the tower top for a vertical stroke to the tower is higher than that characterized by the direct method for more than 25 %. On the other hand, the tower surge impedance representing the current splitting ratio for a stroke to mid-span or to an adjacent tower is about 10 % lower than that characterized by the direct method.

Thirdly, the surge characteristics of an earth-wired tower struck by a vertical lightning stroke are studied with the help of NEC-2. Particularly, the transient behavior of the tower footing impedance, and that of the coupling coefficient between an earth wire and a phase conductor, which influence the insulator voltages, are investigated. The tower footing impedance exhibits initially a high value, which gradually falls off to the value of the footing resistance. This apparent high footing impedance is physically ascribable to the distortion of the current wave propagating a tower. The distortion is partly caused by the strong axial electric field associated with the fast-front current wave itself, and is partly caused by the base-broadened structure of double-circuit towers, where a tower and its image behave as a non-homogeneous waveguide. The coupling coefficient is much lower than that in the TEM mode when it is evaluated at the moment of the peak of the insulator voltage even if a ramp current having a rise time of as long as 2 μs is injected. This effect is due to the transient upward electric field generated by the fast-front tower current, which cancels the downward field produced by the charge in the earth wire.

Finally, a new procedure to determine the circuit parameters of the multistory tower model for the EMTP multi-conductor analysis, on the basis of the measured insulator voltages of an earth-wired tower, is proposed. The multistory model employing the proposed parameters can well reproduce the measured insulator voltages. The recommended surge impedance of the top of the multistory tower model is 200 Ω for a typical earth-wired double-circuit tower, which is about 35 % higher than that of the same tower without earth wires. This higher value takes account of the initially low coupling coefficients.

Contents

Chapter 1

Introduction

1.1 Lightning Surge Analysis of Overhead Transmission Lines

For overhead power transmission lines, lightning is the primary cause of unscheduled interruptions. The lightning overvoltages on overhead transmission lines are caused by either direct strokes to the phase conductors, called shielding failures, or back-flashovers of the tower insulation associated with lightning strokes to the tower top or the earth wires. The number of shielding failures is estimated to be only about 4 % of all flashovers [1], for instance, on 500 kV double-circuit transmission lines. Almost all the remainders are the back-flashovers. Indirect lightning strokes, striking the ground in the vicinity of overhead lines, also induce transient voltages on the lines, however, the magnitude of induced voltages does not threaten the insulation of transmission lines.

In analyzing the lightning performance of overhead power transmission lines and substations, the statistical data of lightning such as the ground flash density and the stroke peak current distributions are essential, therefore, competent observations have been performed with lightning location systems [2][3]. On the other hand, the lightning surge characteristics of transmission-line components are also important, and therefore various studies have been done to measure the characteristics of the line components and to develop their equivalent circuit models for the traveling wave analysis [4][5] or the EMTP simulations [6][7]. Among the transmission line components, following characteristsics are particularly important since they contribute directly to back-flashovers.

(i) Tower surge characteristics.

(ii) Tower footing impedance characteristics.

(iii) Surge corona.

(iv) Air gap flashover characteristics.

Tower surge characteristics and tower footing impedance characteristics contribute to the insulator voltages during a lightning hit. The impulse corona from earth wires reduces the insulator voltages by increasing the coupling to phase conductors and by decreasing the surge impedance of earth wires. Air gap flashover characteristics directly dominate the back-flashovers. Among them, the most fundamental factor is probably tower surge characteristics including the footing impedance characteristics in the linear region.

The electromagnetic field around a tower struck by a lightning stroke changes dynamically while a traveling wave makes several round-trips in the tower. During this interval, the waveforms of insulator voltages vary complexly. This time-dependent or frequency-dependent characteristics cannot be represented by a simple lossless line terminated by the footing resistance, unless the rise time of a lightning current is much less than the round-trip time of a traveling wave in the tower. Particularly for such tall structures as EHV or UHV double-circuit towers, the characteristics become more dominant owing to the longer round-trip time of a traveling wave in the tower (Fig. 1.1). An agreement on the interpretation of this phenomenon, however, has not been reached yet.

This kind of studies is classified into two stages. The first stage is to understand the physical characteristics mainly by carrying out experiments. The second stage is to develop a numerical method that can reproduce the obtained physical characteristics for the traveling wave analysis or the EMTP analysis.

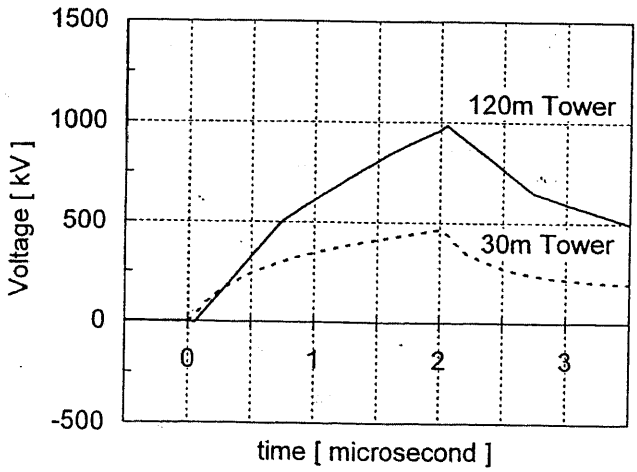

Fig. 1.1 Voltage waveforms of upper-phase insulators of a 120 m and a 30 m high tower computed by EMTP with the multistory tower model [9] employing the same fundamental parameters for the injection of the ramp current having 2 μs rise time and 30 kA magnitude.

1.2 Evaluation Methods of Tower Surge Characteristics

There have been three representative methods to evaluate the transient characteristics of a tower as follows.

(i) Measurements on full-sized towers [8]-[13].

(ii) Measurements on reduced-scale models [14]-[18].

(iii) Theoretical studies on simplified geometories [19]-[22].

Measurements on full-sized towers are classified into those by the direct method [8]-[11] and those by the refraction or the reflection method [12][13]. In the measurement by the direct method, the step current is injected into the tower top by a pulse current generator placed at the tower top, and the voltage between the tower top and a voltage measuring wire, or across an insulator string is measured by a voltage divider. This method is straightforward in evaluating the insulator voltage when the tower is struck by a lightning stroke, and the influence of the ground conductivity is automatically incorporated. Therefore, the tower parameters employed in the evaluation of lightning performance in Japan [4][7] are based on the measurements by this method. It is, however, difficult to carry out this kind of experiments in the ideal arrangement where a current lead wire is stretched vertically above the tower top to simulate a lightning channel, owing to its scale. The geometrical arrangement in measurements so far [8]-[11], therefore, has been different from the incident of lightning hitting a tower. In the measurement by the refraction method, a wire to guide a rectangular pulse current is connected to the top of a tower under measurement, and the refracted or the reflected wave on the measuring wire is observed to evaluate the transient impedance at the tower top. This method is considered valid in evaluating refraction and reflection of surges, associated with mid-span strokes or strokes to adjacent towers, at the connecting point of the tower and the earth wires. The tower surge characteristics evaluated by this method, therefore, should be distinguished from those by the direct method.

Measurements of lightning surges generated by natural or rocket-triggered lightning strokes on a 275 kV test transmission line [23]-[25] are also included in the above category. They have contributed to the verification of the performance of transmission-line surge arresters and to that of air gap flashover models [26][27]. Since the tower under measurements has a non-standard

shape and the lines sag extraordinarily, determined parameters for this tower may not apply to other typical double-circuit towers.

Measurements on reduced-scale models [14]-[18] are more economical than those on full-sized towers, and are flexible in setting up various experimental arrangements. It is, however, not easy to maintain the accuracy of the measurement, particularly in the measurement by the direct method [14]-[16], since the geometrical size of the measuring devices is large relative to the measured system. Results measured on reduced-scale models, therefore, have hardly been employed in the practical calculation of the lightning performance of transmission lines.

Theoretical studies drawing upon various simplifying approximations [19]-[22] have continuously been performed, however, the derived simple formulas for a cylinder do not agree with the corresponding experimental results [28]. Although this approarch is useful in understanding the phenomenon, it is invalid for the accurate evaluation of the dynamic electromagnetic behavior of a three-dimensional system struck by lightning.

1.3 Electromagnetic Modeling Codes

For the accurate analysis of the dynamic electromagnetic field around a complex tower system struck by lightning, electromagnetic modeling codes are appropriate. Of many available codes, those based on the Method of Moments (MoM) [29] are probably best suitable for the electromagnetic analysis of a tower system since they have widely and successfully been used in analyzing thin-wire antennas or scattering structures [30], and a tower system can be regarded as a thin-wire antenna.

The MoM needs to model only the metal structure of interest, and does not need to model the space around it. Long wires are, therefore, easily modeled. This is the advantage compared with the Finite Difference Time Domain (FDTD) Method [31] that may also be applicable to this problem. The MoM is a frequency domain technique, therefore, Fourier transform and inverse Fourier transform are used to analyze time-varying response. The MoM requires that the entire structure be divided into wire segments that must be small compared to the wavelength. Once the model is defined, an excitation is imposed as a voltage source or a plane wave on one of the wire segments. The MoM is to determine the current on every segment due to the source and all the other currents by numerically solving the electric field integral equation. Once these

currents are known, the electric field at any point in space is determined from the sum of the contributions of all the wire segments. The MoM allows discrete circuit elements to be inserted into a model by simply defining the impedance desired on any given wire segment.

Pioneering work in applying an originally developed MoM-based code to the analysis of power system transients was done by Grcev *et al.* [32] and by Kato *et al.* [33]. The former applied it to the analysis of grounding grids and the latter did to the analysis of towers. Although the computed results of the latter did not agree well with the corresponding experimental results, this work is worth admiring.

As a MoM-based code, the author chooses the Numerical Electromagnetic Code (NEC) [34] for the present work. This code was developed at the Lawrence Livermore National Laboratory, California, under the sponsorship of the Naval Ocean Systems Center and the Air Force Weapons Laboratory. Although the latest version is NEC-4 [35], it is available only to the citizens of the United States and Canada, or to the users who are licensed from Lawrence Livermore National Laboratory [36]. Therefore, the author employs NEC-2 developed in 1980 that is easily available. The information on the history and availability of the NEC-MoM codes is found in Appendix A.

1.4 Objectives and Scope of Thesis

The purposes of this work are to clarify the surge characteristics of a transmission tower by analyzing the electromagnetic field around it with the help of NEC-2, and to develop a equivalent circuit of a tower for EMTP multi-conductor analyses.

In chapter 2, the numerical solution of the electric field integral equations used in NEC-2 is outlined, and the validity and the accuracy of NEC-2 when it is applied to the electromagnetic field analysis of tower surge response are demonstrated by comparison with experimental results. In chapter 3, two principal measuring methods of tower surge impedance are briefly explained, and then the effects of the measuring methods and the arrangements of the measuring wires on the evaluated tower surge impedance are studied by NEC-2. On the basis of the obtained results, the surge impedance of typical double-circuit towers is estimated. In chapter 4, the lightning surge characteristics of an earth-wired tower are studied with the help of NEC-2. Particularly, the transient behavior of the tower footing impedance, and that of the coupling

coefficient between an earth wire and a phase conductor, which influence the voltage across an insulator, are investigated. In chapter 5, tower models proposed so far are reviewed with emphasis on their performance in reproduction of measured waveforms of insulator voltages. Then, a new procedure to determine the parameters of the multistory tower model for EMTP multi-conductor analyses on the basis of the measured insulator voltages on an earth-wired tower is proposed. Finally, in chapter 6, the results of the present work are summarized.

Chapter 2

Application of NEC-2 Code to the Analysis of Tower Surge Response

The purpose of this chapter is to demonstrate the validity and the accuracy of NEC-2 when it is applied to the electromagnetic field analysis of tower surge response. The electric field integral equation used in NEC-2, its derivation, and the numerical method are first outlined. Guidelines for modeling structures with this code follow. Finally, the applicability of NEC-2 to the transient analysis of the impedance of a transmission tower is verified by comparison with experimental results.

2.1 Electric Field Integral Equation

The form of the electric field integral equation used in NEC-2 [34] follows from an integral representation for the electric field of a volume current distribution $\boldsymbol{J}_V$,

$$\boldsymbol{E}(\boldsymbol{r}) = \frac{-j\eta}{4\pi k}\int_V \boldsymbol{J}_V(\boldsymbol{r}')\cdot\bar{\bar{G}}(\boldsymbol{r},\boldsymbol{r}')dV', \tag{2.1}$$

where

$$\begin{aligned}\bar{\bar{G}}(\boldsymbol{r},\boldsymbol{r}') &= (k^2\bar{\bar{I}} + \nabla\nabla)g(\boldsymbol{r},\boldsymbol{r}'),\\ g(\boldsymbol{r},\boldsymbol{r}') &= exp(-jk|\boldsymbol{r}-\boldsymbol{r}'|)/|\boldsymbol{r}-\boldsymbol{r}'|,\\ k &= \omega\sqrt{\mu_0\epsilon_0} \quad , \quad \eta = \sqrt{\mu_0/\epsilon_0}\end{aligned}$$

and the time convention is $exp(j\omega t)$. $\bar{\bar{I}}$ is the identity dyad ($\hat{\boldsymbol{x}}\hat{\boldsymbol{x}}+\hat{\boldsymbol{y}}\hat{\boldsymbol{y}}+\hat{\boldsymbol{z}}\hat{\boldsymbol{z}}$). When the current distribution is limited to the surface of a perfectly conducting body, equation (2.1) becomes

$$\boldsymbol{E}(\boldsymbol{r}) = \frac{-j\eta}{4\pi k}\int_S \boldsymbol{J}_S(\boldsymbol{r}')\cdot\bar{\bar{G}}(\boldsymbol{r},\boldsymbol{r}')dS', \tag{2.2}$$

with $\boldsymbol{J}_S$ the surface current density. The observation point $\boldsymbol{r}$ is restricted to be off the surface S so that $\boldsymbol{r} \neq \boldsymbol{r}'$.

If $\boldsymbol{r}$ approaches S as a limit, equation (2.2) becomes

$$\boldsymbol{E}(\boldsymbol{r}) = \frac{-j\eta}{4\pi k} \oint_S \boldsymbol{J}_S(\boldsymbol{r}') \cdot \bar{\bar{G}}(\boldsymbol{r}, \boldsymbol{r}') dS', \tag{2.3}$$

where the principal value integral $\oint$ is indicated since $g(\boldsymbol{r}, \boldsymbol{r}')$ is now unbounded.

An integral equation for the current induced on S by an incident field $\boldsymbol{E}_{inc}$ can be obtained from equation (2.3) and the boundary condition for $\boldsymbol{r} \in S$,

$$\boldsymbol{n}(\boldsymbol{r}) \times [\ \boldsymbol{E}_{scat}(\boldsymbol{r}) + \boldsymbol{E}_{inc}(\boldsymbol{r})\ ] = 0, \tag{2.4}$$

where $\boldsymbol{n}(\boldsymbol{r})$ is the unit normal vector of the surface at $\boldsymbol{r}$ and $\boldsymbol{E}_{scat}$ is the field due to the induced current $\boldsymbol{J}_S$. Substituting equation (2.3) for $\boldsymbol{E}_{scat}$ yields the integral equation,

$$-\boldsymbol{n}(\boldsymbol{r}) \times \boldsymbol{E}_{inc}(\boldsymbol{r}) = \frac{-j\eta}{4\pi k} \boldsymbol{n}(\boldsymbol{r}) \times \oint_S \boldsymbol{J}_S(\boldsymbol{r}') \cdot (k^2 \bar{\bar{I}} + \nabla\nabla) g(\boldsymbol{r}, \boldsymbol{r}') dS'. \tag{2.5}$$

The vector integral in equation (2.5) can be reduced to a scalar integral equation when the conducting surface S is that of a cylindrical thin wire, thereby making the solution much easier. The assumptions applied to a thin wire, known as the thin-wire approximation, are as follows:

(i) Transverse currents relative to axial currents on the wire can be neglected.

(ii) The circumferential variation in the axial current can be neglected.

(iii) The current can be represented by a filament on the wire axis.

(iv) The boundary condition on the electric field need be enforced in the axial direction only.

These approximations are valid as far as the wire radius is much less than the wavelength and much less than the wire length.

From assumptions (i), (ii) and (iii), the surface current $\boldsymbol{J}_S$ on a wire of radius a can be replaced by a filamentary current I,

$$I(s)\hat{\boldsymbol{s}} = 2\pi a \boldsymbol{J}_S(\boldsymbol{r}),$$

where s is the distance parameter along the wire axis at $\boldsymbol{r}$, and $\hat{\boldsymbol{s}}$ is the unit vector tangent to the wire axis at $\boldsymbol{r}$.

Equation (2.5) then becomes

$$-\boldsymbol{n}(\boldsymbol{r}) \times \boldsymbol{E}_{inc}(\boldsymbol{r}) = \frac{-j\eta}{4\pi k} \boldsymbol{n}(\boldsymbol{r}) \times \int_L I(s')(k^2 \hat{\boldsymbol{s}}' - \nabla \frac{\partial}{\partial s'}) g(\boldsymbol{r}, \boldsymbol{r}') ds', \tag{2.6}$$

where the integration is over the length of the wire. Enforcing the boundary condition in the axial direction reduces equation (2.6) to the scalar equation,

$$-\hat{s}\cdot\boldsymbol{E}_{inc}(\boldsymbol{r}) = \frac{-j\eta}{4\pi k}\int_L I(s')(k^2\hat{s}\cdot\hat{s}' - \frac{\partial^2}{\partial s\partial s'})g(\boldsymbol{r},\boldsymbol{r}')ds', \tag{2.7}$$

since $\boldsymbol{r}'$ is now the point at s' on the wire axis while $\boldsymbol{r}$ is a point at s on the wire surface $|\boldsymbol{r}-\boldsymbol{r}'| \geq a$ and the integrand is bounded.

The electric field integral equation is easily extended to imperfect conductors by modifying the boundary condition from equation (2.4) to

$$\boldsymbol{n}(\boldsymbol{r})\times[\ \boldsymbol{E}_{scat}(\boldsymbol{r}) + \boldsymbol{E}_{inc}(\boldsymbol{r})\ ] = Z_S(\boldsymbol{r})[\ \boldsymbol{n}(\boldsymbol{r})\times\boldsymbol{J}_S(\boldsymbol{r})\ ]. \tag{2.8}$$

where $Z_S(\boldsymbol{r})$ is the surface impedance at $\boldsymbol{r}$ on the conducting surface. For a wire, the boundary condition is

$$\hat{s}\cdot[\ \boldsymbol{E}_{scat}(\boldsymbol{r}) + \boldsymbol{E}_{inc}(\boldsymbol{r})\ ] = Z_L(s)I(s), \tag{2.9}$$

with $Z_L(s)$ the impedance per-unit-length at s.

2.2 Numerical Solution by the Method of Moments

The integral equation (2.7) is solved numerically in NEC-2 by the method of moments [29]. This method applies to a general linear-operator equation,

$$Lf = e, \tag{2.10}$$

where f is an unknown response, e is a known excitation, and L is a linear operator (an integral operator in the present case). The unknown function f may be expanded in a sum of basis functions, f_j, as

$$f \simeq \sum_{j=1}^{N}\alpha_j\cdot f_j. \tag{2.11}$$

A set of equations for the coefficients α_j are then obtained by taking the inner product of equation (2.10) with a set of weighting functions, $\{\ w_i\ \}$,

$$< w_i, Lf > = < w_i, e > \qquad i = 1,\ldots,N. \tag{2.12}$$

Due to the linearity of L, equation (2.11) substituted for f yields,

$$\sum_{j=1}^{N}\alpha_j < w_i, Lf_j > = < w_i, e > \qquad i = 1,\ldots,N. \tag{2.13}$$

This equation can be written in matrix notation as

$$[G][A] = [E], \tag{2.14}$$

where

$$G_{ij} =< w_i, Lf_j >, \qquad A_j = \alpha_j, \qquad E_i =< w_i, e > .$$

The solution is then

$$[A] = [G]^{-1}[E].$$

For the solution of equation (2.7), the inner product is defined as

$$< f, g >= \int_S f(\boldsymbol{r})g(\boldsymbol{r})dS,$$

where the integration is over the structure surface. Various choices are possible for the weighting functions $\{ w_i \}$ and basis functions $\{ w_i \}$. When $w_i = f_j$, the procedure is known as Galerkin's method. In NEC-2, the basis and weighting functions are different, and w_i are chosen as a set of delta functions

$$w_i(\boldsymbol{r}) = \delta(\boldsymbol{r} - \boldsymbol{r}_i),$$

with $\{ \boldsymbol{r}_i \}$ a set of points on the conducting surface. The result is a point sampling of the integral equations known as the collocation method of solution. Wires are divided into short straight segments with a sample point at the center of each segment.

The choice of basis functions is very important for an efficient and accurate solution. In NEC-2, the support of f_i is restricted to a localized subsection of the surface near $\boldsymbol{r}_i$. This choice simplifies the evaluation of the inner-product integral and ensures that the matrix G will be well conditioned. For finite N, the sum of f_j cannot exactly equal to a general current distribution.

Wires in NEC-2 are modeled by short straight segments with current on each segment represented by three terms — a constant, a sine function and a cosine function. This expansion has been shown to provide rapid solution convergence. It has the added advantage that the fields of the sinusoidal currents are easily evaluated in a closed form. The amplitudes of the constant, sine, and cosine terms are related such that their sum satisfies physical conditions on the local behavior of current and charge at the segment ends.

The total current on segment number j in NEC-2 has the form

$$I_j = A_j + B_j \sin k(s - s_j) + C_j \cos k(s - s_j), \tag{2.15}$$

$$|s - s_j| < \frac{\Delta_j}{2},$$

where s_j is the value of s at the center of segment j and Δ_j is the length of segment j. Of the three unknown constants A_j, B_j and C_j, two are eliminated by local conditions on the current leaving one constant, related to the current amplitude, to be determined by the matrix equation. The local conditions are applied to the current and to the linear charge density, q, which is related to the current by the equation of continuity

$$\frac{\partial I}{\partial s} = -j\omega q. \tag{2.16}$$

At a junction of two segments with a uniform radius, the obvious condition is that the current and charge are continuous at the junction. At a junction of two or more segments with unequal radii, the continuity of current is generalized to Kirchoff's current law that the sum of currents into the junction is zero. The total charge in the vicinity of the junction is assumed to distribute itself on individual wires according to the wire radii, neglecting local coupling effects.

2.3 Structure Modeling Guidelines

A wire segment is defined by the coordinates of its two end points and its radius. Modeling a wire structure with segments involves both geometrical and electrical factors. Geometrically, the segments should follow the paths of conductors as closely as possible, using a piece-wise linear fit on curves.

The main electrical consideration is on the segment length ΔL relative to the wavelength λ. Generally, ΔL should be less than about 0.1 λ at the desired frequency. Somewhat longer segments may be acceptable on long wires with no abrupt changes while shorter segments, 0.05 λ or less, may be needed in modeling critical regions of an antenna. The size of the segmemts determines the resolution in solving the current on the model since the current is computed at the center of each segment. Extremely short segments, less than about $10^{-3}\lambda$, should also be avoided since the similarity of the constant and cosine components of the current expansion leads to numerical inaccuracy.

The wire radius, a, relative to λ is ristricted. In the thin-wire kernel, only currents in the axial direction on a segment are considered, and there is no allowance for variation of the current around the wire circumference. The acceptability of this approximation depends on both the

value of a/λ and the tendency of the excitation to produce circumferential current or current variation. Unless $2\pi a/\lambda$ is much less than 1, the validity of these approximations should be considered.

The accuracy of the numerical solution for the dominant axial current is also dependent on $\Delta L/a$. It must be greater than about 8 to limit errors less than 1 %, since small values of it may result in extraneous oscillations in the computed current near free wire ends, voltage sources, or lumped loads.

The current expansion used in NEC-2 enforces conditions on the current and charge density along wires, at junctions, and at wire ends. For these conditions to be applied properly, segments that are electrically connected must have coincident end points. If segments intersect other than at their ends, the NEC-2 code will not allow current to flow from one segment to the other.

The angle of the intersection of wire segments in NEC-2 should be as large as possible. An acute angle may decrease accuracy.

Other rules for the segment model follow:

- Segments may not overlap since the division of current between two overlapping segments is indeterminate. Overlapping segments may result in a singular matrix equation.
- A large radius change between connected segments may decreace accuracy; particularly, with small $\Delta L/a$. The problem may be reduced by making the radius change in steps over several segments.
- A segment is required at each point where a network connection or voltage source will be located. This may seem contrary to the idea of an excitation gap as a break in a wire. A continuous wire across the gap is needed, however, so that the required voltage drop can be specified as a boundary condition.
- It is safe to specify that wires should be several radii apart.

Several options are available in NEC-2 for modeling an antenna over a ground plane. For a perfectly conducting ground, the code generates an image of the structure reflected on the ground surface. The image is exactly equivalent to a perfectly conducting ground and results in solution accuracy comparable to that for a free-space model. Structures may be close to the

ground or contacting it in this case. However, for a horizontal wire with radius a, and height h to the wire axis, $(h^2 + a^2)^{\frac{1}{2}}$ should be greater than about 10^{-6} wavelength. Furthermore, the height should be at least several times the radius for the thin-wire approximation to be valid.

A finitely conducting ground can be modeled by the Sommerfeld - Norton approximation. It should be noted that NEC-2 can model wires over lossy ground but it cannot model wires buried in the ground. Although NEC-4 [35], the latest version of the NEC-MoM codes, can model buried wires, it is available only to the citizens of the United States and Canada, or to the users who are licensed from Lawrence Livermore National Laboratory. The information on the NEC-MoM codes is found in Appendix A.

2.4 Application to the Analysis of Tower Surge Response

The validity and the accuracy of NEC-2, when it is applied to the electromagnetic field analysis of tower surge response, are verified by comparison with experiments. For the comparison, a series of well-documented measurements of the surge characteristics of simple structures reported by Hara *et al.* [37][38] are chosen. In the experiments, surge responses of such structures of 3 m in height as shown in Fig. 2.1 were measured. The vertical single conductor in Fig. 2.1 (a) has a radius of 2.5 mm, and the vertical four conductors in Fig. 2.1 (b) has a radius of 16.5 mm and 404 mm apart. The experimental setup on a metal plane is shown in Fig. 2.2. A steep-front current having the risetime of 5 ns was injected into a horizontal current lead wire. The current flowing into a structure was measured through a current transformer. The voltage between the top of a structure and a horizontal voltage measuring wire, which was perpendicular to the current lead wire, was measured through a voltage probe. The rise times of the current transformer and the voltage probe are 2 ns and 0.7 ns, respectively, which are fast enough to measure the response of this system.

Since NEC-2 is a computer code in the frequency domain, the Fourier transform and the inverse Fourier transform are used to solve the time-varing electromagnetic fields. The solution process is shown in Fig. 2.3.

For the numerical analysis, the conductor system needs to be modeled with segments according to the modeling guidelines stated in the preceding chapter. It is not difficult to satisfy

recommended conditions except the following one:

$$0.001\lambda < \Delta L < 0.1\lambda.$$

This requirement is too severe to be satisfied exactly, since wider frequency range is needed to investigate the transient characteristics of such a system. By trial and error process, however, the author found the following condition yielding reasonable computation results, which deviated the above recommended condition.

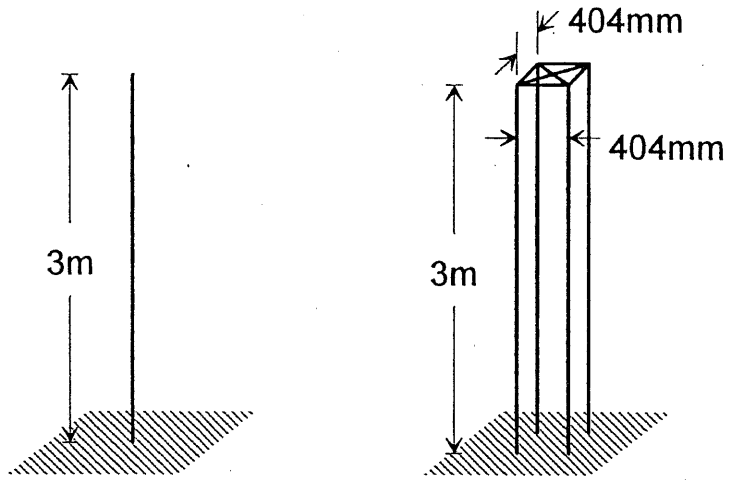

(a) Single conductor. (b) Four parallel conductors.

Fig. 2.1 Structures subject to analysis.

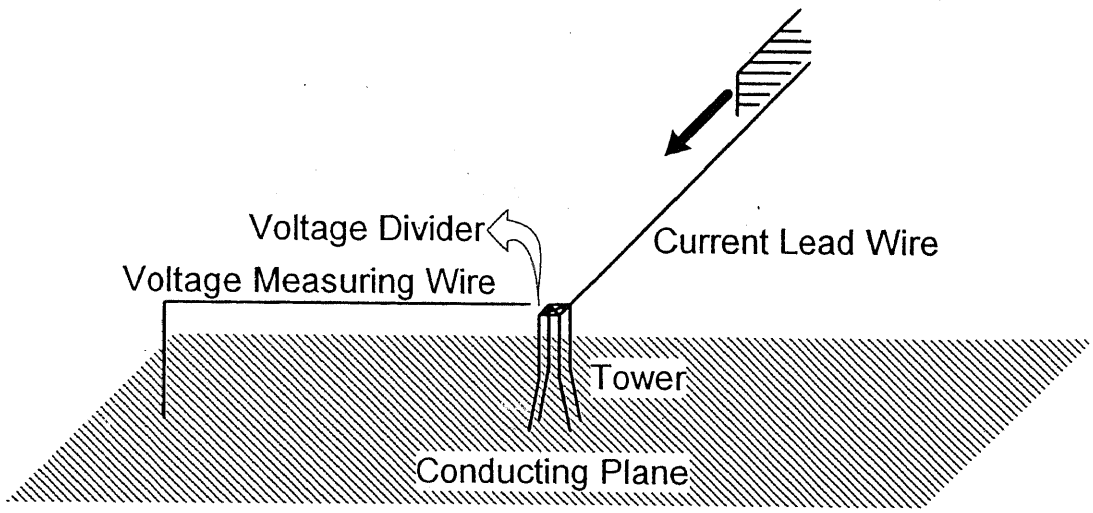

Fig. 2.2 Setup of Hara *et al.*'s experiment [37][38].

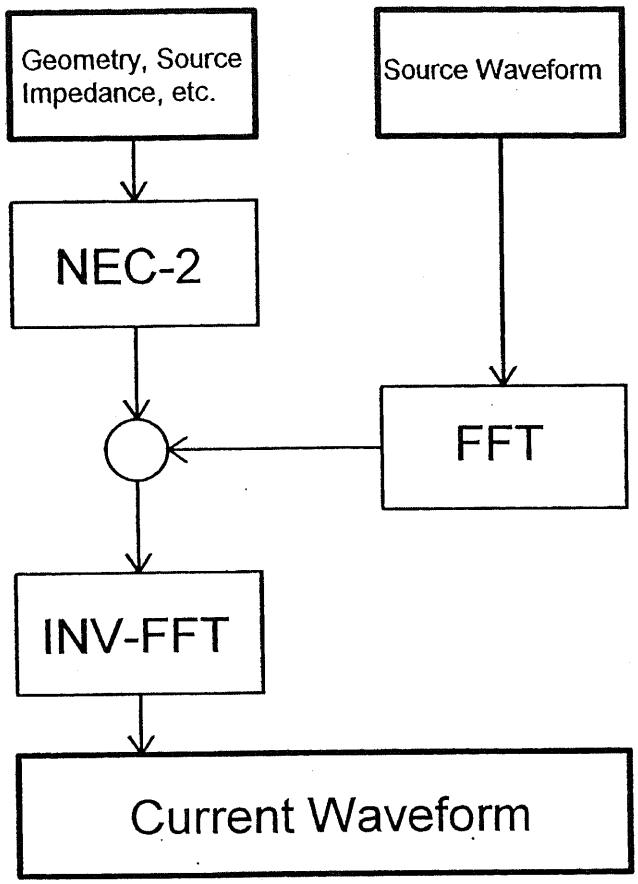

Fig. 2.3 Flow of the solution using NEC-2.

Frequency range : 1.5625 MHz to 0.8000 GHz with 1.5625 MHz increment step

Segment length : 0.202 m to 0.300 m

The above frequency range corresponds to the time range of 0 to 640 ns with 1.25 ns increments. The computation time with a Pentium II 400 MHz processor with 64 MB RAM for the above analyses is within 100 s. The input data to NEC-2 are shown in Appendix A.

To evaluate the voltage of the top of a structure, 10 kΩ resistance was inserted between the top of a structure and the end of the voltage measuring wire, and the waveform of the current flowing through the resistance was calculated. The system of structures under the numerical analysis was postulated to be on the perfectly conducting ground. This postulation is used throughout in this thesis.

Figure 2.4 shows the measured and computed waveforms of the voltage and the current at the top of the single conductor. Figure 2.5 shows those of the four parallel conductors. The computed waveforms agree well with the measured ones. The tower surge impedances calculated from Figs. 2.4 and 2.5 are summarized in Table 2.1, where the tower surge impedance is defined as the ratio of the instantaneous values of the voltage to the current at the moment of the voltage peak. The agreement between the measured and the computed tower surge impedance is also quite well with the maximum difference of only about 5 %.

Through the above comparison between the measured and computed results, the numerical analysis employing NEC-2 is proved to be practical enough to be applied to the investigation of the transient response of towers.

Table 2.1 Measured [37][38] and computed tower surge impedances.

	Experiment	Computation
Single conductor	about 360 Ω	377 Ω
Four conductors	about 120 Ω	125 Ω

If a traveling wave propagates along the tower at the velocity of light, the reflected wave from the ground should return to the tower top after the round-trip time of a traveling wave in the tower, which is 20 ns for the structures in Fig. 2.1. In the both measured and computed results of Figs. 2.4 and 2.5, however, the voltage waveforms reach their peaks about 17 ns after the beginning, which indicates that a negative voltage wave arrives at the top before the arrival of the reflected wave from the ground.

This phenomenon is due to the electromagnetic field of TEM mode illuminating the structure, i.e., the electromagnetic wave associated with a traveling wave in the current lead wire arrives at the structure foot simultaneously with the arrival at the top of a structure, and a negative voltage wave is induced at the structure foot before the occurrence of the reflection of the traveling wave propagating down from the top of the structure. This induced wave is observed in the current waveforms in Figs. 2.4 and 2.5 as the gradual increase of the current before 20 ns. This phenomenon is studied further in the following chapter.

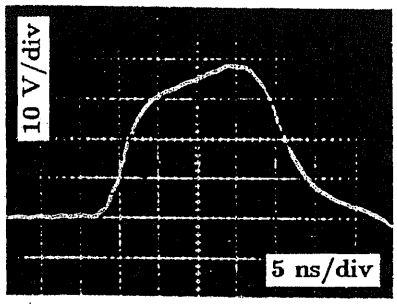

(a) Measured voltage.

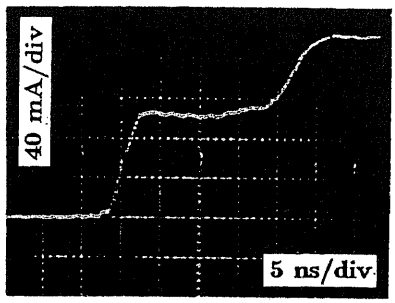

(b) Measured current.

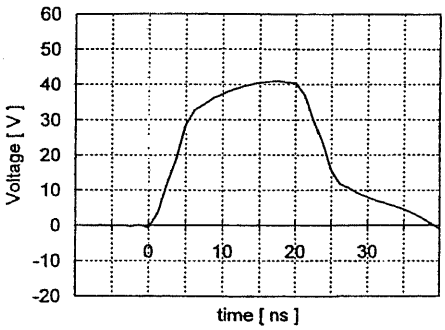

(c) Computed voltage.

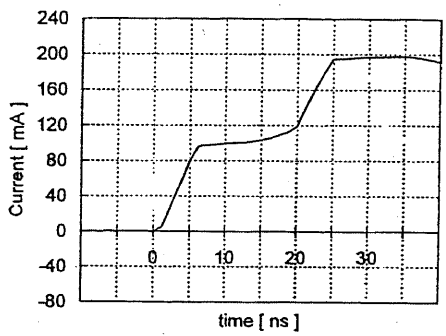

(d) Computed current.

Fig. 2.4 Measured (a)(b) [37] and computed (c)(d) waveforms for the single conductor.

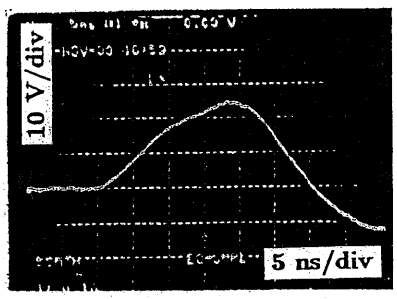

(a) Measured voltage.

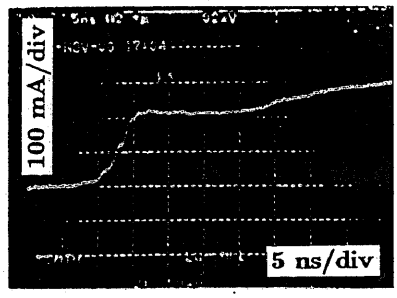

(b) Measured current.

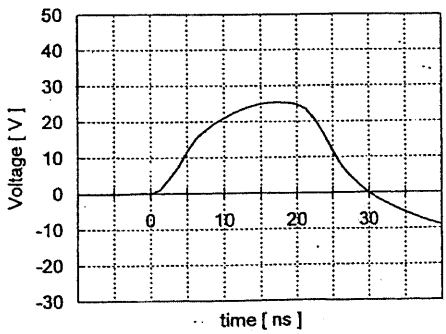

(c) Computed voltage.

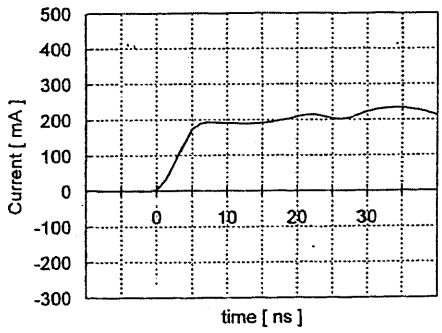

(d) Computed current.

Fig. 2.5 Measured (a)(b) [38] and computed (c)(d) waveforms for the four parallel conductors.

Chapter 3

Evaluation of Measuring Methods of Tower Surge Impedance

For measuring the surge impedance of towers, two principal methods have been used: one is the direct method, and the other is the refraction or the reflection method. Although these two methods are quite different, the difference has not been fully discussed yet. In this chapter, measuring methods are briefly explained, and then the effects of the measuring methods and the arrangements of the measuring wires on the evaluated tower surge impedance are studied with the help of NEC-2. On the basis of obtained results and various experimental results, the surge impedance of typical double-circuit transmission towers is estimated.

3.1 Measuring Methods of Tower Surge Impedance

In the measurement by the direct method [14][8], the step current is injected into the tower top, and the voltage between the tower top and a voltage measuring wire, or the voltage across an insulator string is measured by a voltage divider as illustrated in Fig. 3.1. The tower top voltage or the insulator voltage measured by this method gradually rises until the reflected wave from the ground arrives, and then it decreases. The tower surge impedance is defined as the ratio of the instantaneous value of the voltage to the current flowing into the tower at the moment of the voltage peak. This method is straightforward in evaluating the insulator voltage when the tower is struck by a lightning stroke. In the measurement at an actual tower, however, it is difficult to stretch a current lead wire vertically from the tower top. Therefore, the geometrical arrangements in measurements so far are somewhat different from the incident of lightning striking a tower, where the current lead wire acts as a vertical lightning channel.

In the measurement by the refraction or the reflection method [12][17], a wire to guide a steep-front current wave is connected to the top of a tower under measurement, and the refracted or the reflected wave on the measuring wire is observed to estimate the transient impedance at the

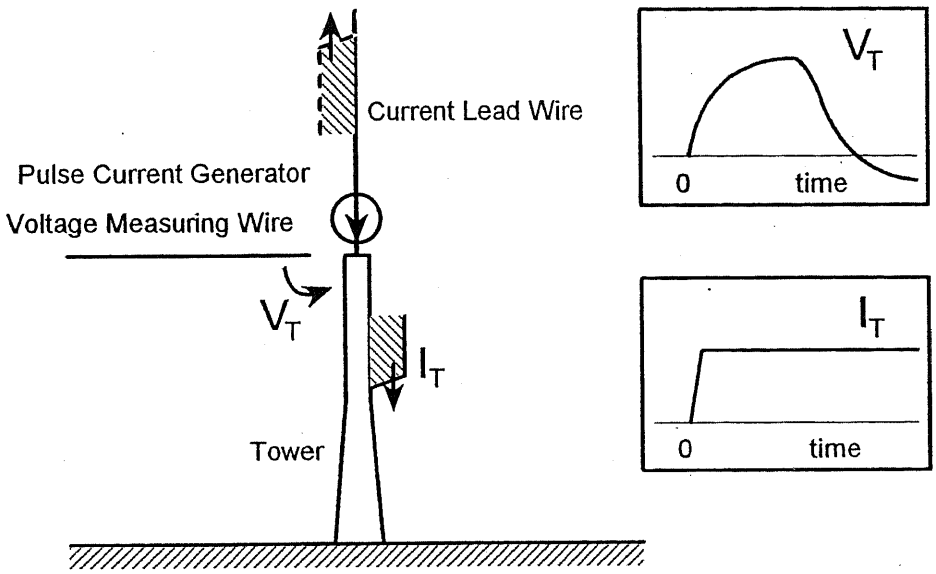

Fig. 3.1 Simplified diagram of the measurement by the direct method, and the characterized response of a tower.

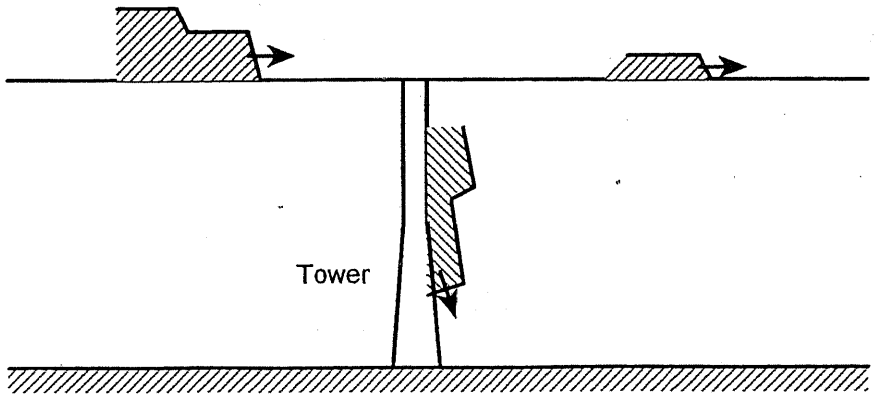

Fig. 3.2 Simplified diagram of the measurement by the refraction or the reflection method, and the characterized response of a tower.

or tower top. This method is considered valid in evaluating refraction and reflection of surges, associated with mid-span strokes or strokes to adjacent towers, at the connecting point of the tower and the earth wires. The tower surge impedance characterized by this method is qualitatively different from the transfer impedance characterized by the direct method, therefore, the value by the refraction method does not necessarily agree with that by the direct method.

3.2 Evaluation of Direct Method

3.2.1 Influence of the Arrangement of Current Lead Wire

Figure 3.3 illustrates the arrangements for the numerical analysis simulating the measurement by the direct method. The numerical analysis is carried out in the three arrangements of the current lead wire: (i) vertical, (ii) horizontal and perpendicular to a horizontal voltage measuring wire, and (iii) horizontal and in extension of a voltage measuring wire. Each wire is 360 m in length and 0.1 m in radius. A rectangular pulse current generator having the internal impedance of 5 kΩ is placed on the tower top and connected to the current lead wire. In this thesis, the tower top voltage is defined as the voltage between the tower top and the voltage measuring wire, and it is evaluated through the current flowing a 100 kΩ resistive element inserted between them.

Figure 3.4 (a) illustrates the tower structure subject to analysis. It is composed of four main poles. Each pole has variable radius illustrated in Fig. 3.4 (b), and is directly connected to the perfectly conducting plane. This model tower simulates the structure of double-circuit transmission towers in Japan. This simple structure allows accurate numerical analysis and is convenient to study the effects of measuring wires, although its surge impedance is higher than a model tower with crossarms and slant elements.

For the numerical analysis, the conductors of the system are divided into 10 m or 12 m segments. Computation is carried out in the frequency range of 39.06 kHz to 20.00 MHz with the increment step of 39.06 kHz. This corresponds to the time range of 0 to 25.6 μs with 0.05 μs increments. The computation time with a Pentium 400 MHz processor with 64 MB RAM is about 70 seconds for the above case.

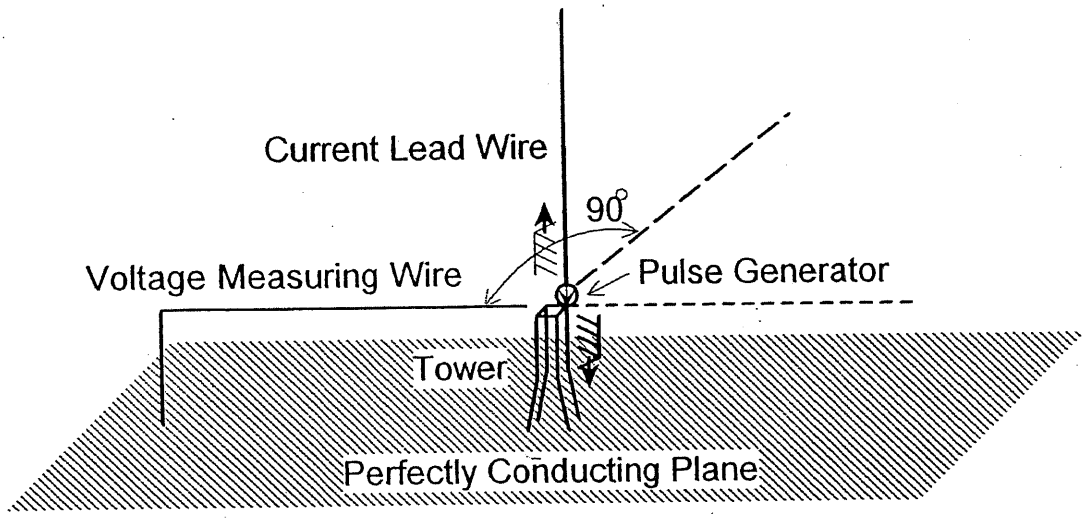

Fig. 3.3 Arrangements for the measurement by the direct method, where a pulse current generator is placed on the tower top.

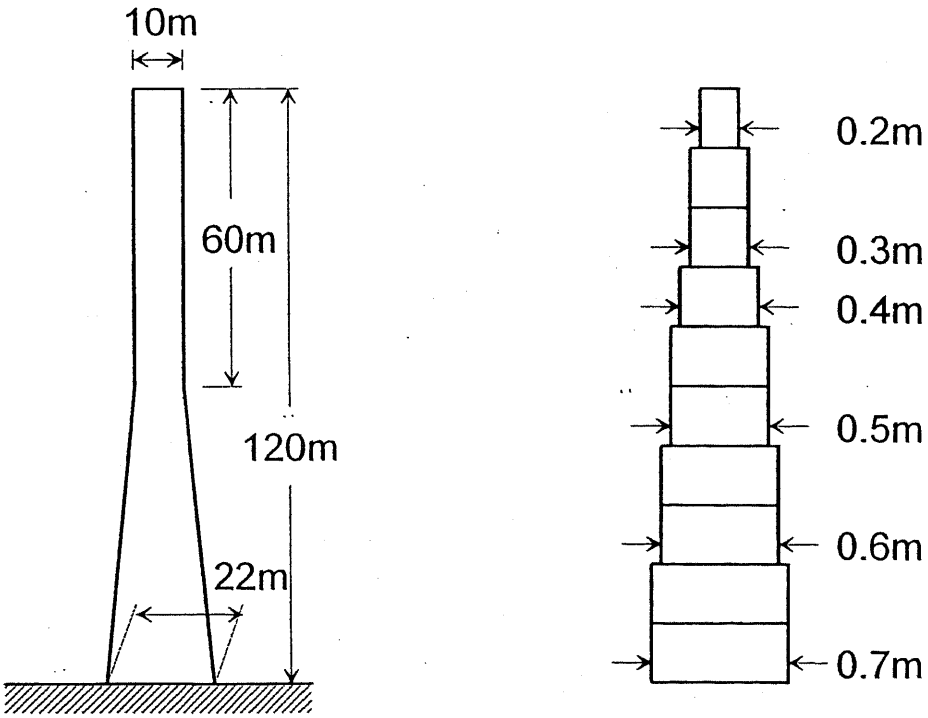

(a) Base-broadened four poles. (b) Detail of the main pole.

Fig. 3.4 The structure of the model tower subject to analysis.

The computed waveforms of the tower top voltage and the injected current are shown in Fig. 3.5. The solid line expresses the case (i), the broken line does the case (ii), and the dotted line does the case (iii). The voltage waveforms reach their peaks at 0.8 μs after the beginning, which indicates that a traveling wave propagates along the tower with the speed of light. This is because the tower model does not include crossarms [39].

The tower surge impedances evaluated at the moment of the voltage peak from Fig. 3.5 are summarized in Table 3.1. The arrangement of the current lead wire affects the measured tower surge impedance. The value for case (i) is about 10 % and 20 % higher than those for case (ii) and case (iii), respectively.

Figure 3.6 shows the effect of the arrangement of current lead wire on the measured tower surge impedance in detail. A voltage measuring wire is stretched horizontally. In Fig. 3.6 (a), a current lead wire is in a horizontal plane at the height of the tower, and the angle between the current lead wire and the voltage measuring wire is varied from 30° to 180°. The angle of 90° corresponds to the case (ii), and that of 180° does the case (iii). In Fig. 3.6 (b), a current lead wire is in a plane perpendicular to the voltage measuring wire, and the angle between the current lead wire and a horizontal plane at the height of the tower is varied from -60° to 90°.

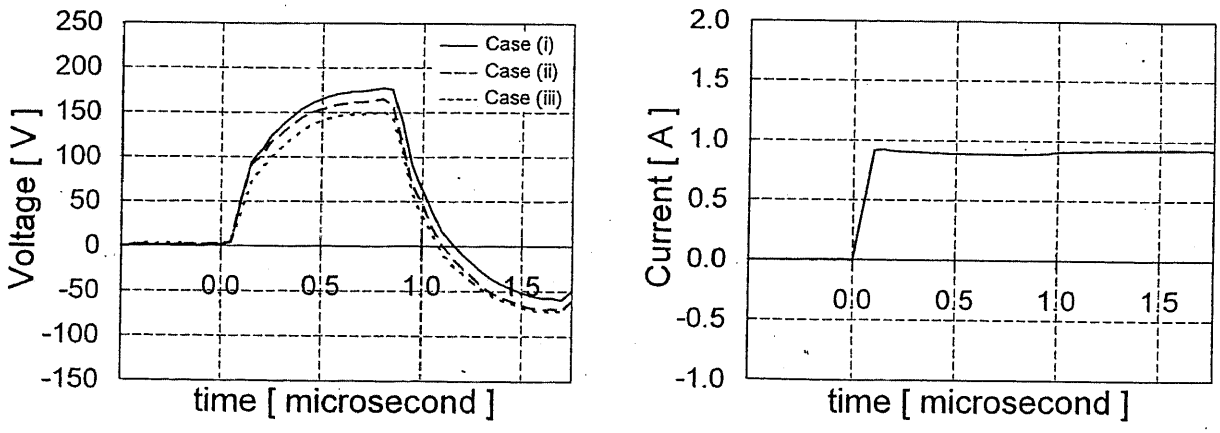

(a) Tower top voltage. (b) Injected current.

Fig. 3.5 Computed waveforms for the base broadened model tower.

Table 3.1 Calculated tower surge impedances characterized by the direct method.

Arrangement	Case (i)	Case (ii)	Case (iii)
Surge impedance	199 Ω	185 Ω	170 Ω

Negative sign of the angle shows that the current lead wire is stretched down to the earth. The angle of 90° corresponds to the case (i), and that of 0° does the case (ii). In both of the figures, the tower surge impedance for the case (ii) is selected as the reference value.

The difference due to the arrangement of the current lead wire becomes greater if the angle between the wires or between the wire and the tower is smaller than 90°.

These results can be used to estimate the tower surge impedance of the standard arrangement with a vertical current lead wire and a horizontal voltage measuring wire from results measured in a different arrangement.

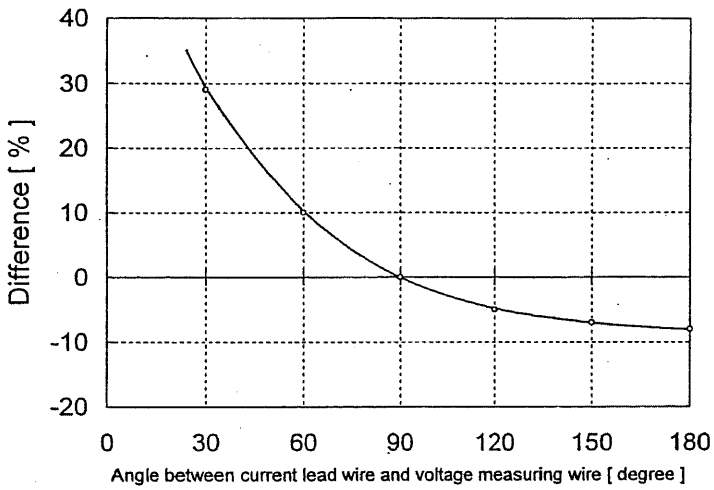

(a) Effect of the angle between the current lead wire and the horizontal voltage measuring wire.

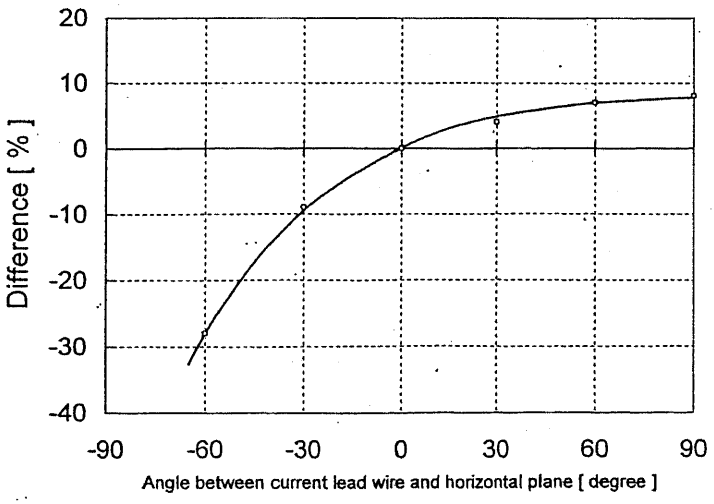

(b) Effect of the angle between the current lead wire and the tower.

Fig. 3.6 Influence of the arrangement of current lead wire on the measured tower surge impedance.

3.2.2 Influence of the Method of Current Injection

An experiment employing a different method of current injection is numerically simulated, where a pulse current generator is inserted into the current lead wire at 150 m from the tower top. The setup for the numerical analysis is illustrated in Fig. 3.7. The cases for the three arrangements of the current lead wire are simulated as the preceding chapter.

The computed waveforms of the tower top voltage and the current flowing into the tower are shown in Fig. 3.8. The solid line corresponds to the case of the vertical current lead wire (case(i)). The voltage waveform reaches its peak at 0.8 μs in this case only, and the value of the tower surge impedance is 205 Ω, which is almost the same as the case for the pulse current generator placed at the tower top.

The broken and dotted lines in Fig. 3.8 are the results for horizontal arrangements of the current lead wire. These two waveforms of the tower top voltage reach their peaks at 0.5 μs, which indicates that a negative voltage wave arrives at the tower top before the arrival of the reflected wave from the ground. In this case, the electromagnetic wave associated with the traveling wave in the current lead wire arrives at the tower foot simultaneously with the arrival at the tower top, and a negative voltage wave is induced at the tower foot before the occurrence of the reflection of the traveling wave propagating down from the tower top. This induction is

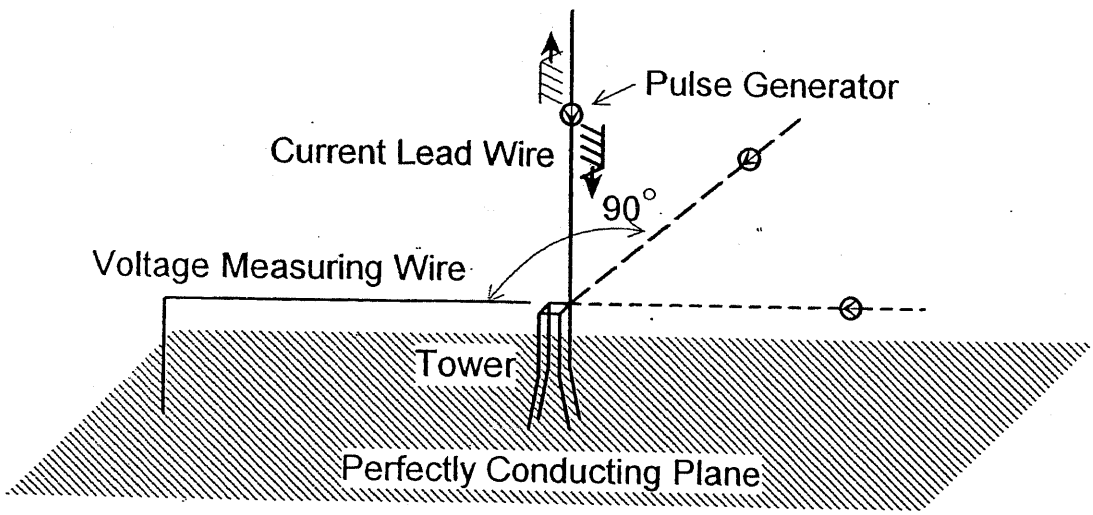

Fig. 3.7 Arrangement for the measurement by the direct method, where a pulse current generator is placed remotely from the tower top.

observed in the dotted waveform in Fig. 3.8 (b) as the gradual increase of the current before 0.8 μs. The tower surge impedances for these cases are evaluated at 0.5 μs. The tower surge impedances calculated from Fig. 3.8 are summarized in Table 3.2.

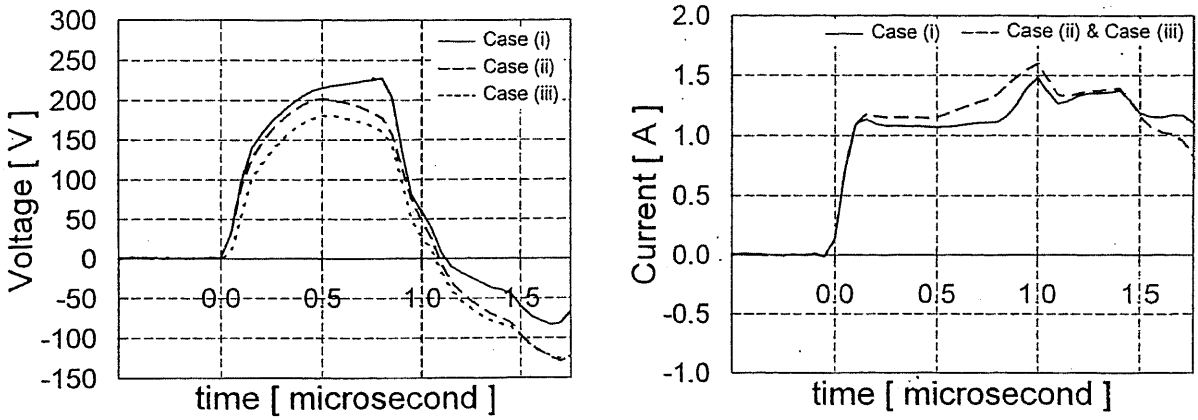

(a) Tower top voltage. (b) Current flowing into the tower.

Fig. 3.8 Computed waveforms for the base broadened model tower.

Table 3.2 Calculated tower surge impedances characterized by the direct method.
(Current injection from distance)

Arrangement	Case (i)	Case (ii)	Case (iii)
Surge impedance	205 Ω	176 Ω	153 Ω

3.3 Evaluation of Refraction Method

Figure 3.9 illustrates schematic diagrams to measure the current splitting ratio between the tower and the earth wire. Figure 3.9 (a) simulates a lightning return stroke to the tower top, Fig. 3.9 (b) does a downward traveling current to the tower top, and Fig. 3.9 (c) does a stroke to mid-span. Measurements employing Fig. 3.9 (c) have been called the refraction method.

In Fig. 3.9 (a), a pulse current generator is placed on the tower top, and is connnected to a long vertical current lead wire, while in Fig. 3.9 (b), a pulse current generator is inserted into the current lead wire at 150 m upward from the tower top. A long earth wire is stretched horizontally. In Fig. 3.9 (c), a pulse current generator is inserted into the earth wire at 150 m left from the tower top.

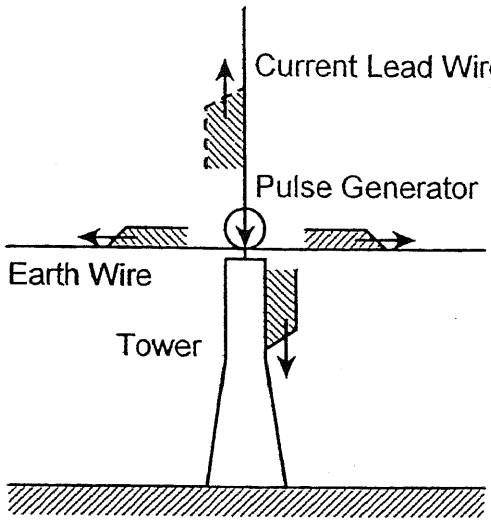

(a) Return stroke to a tower.

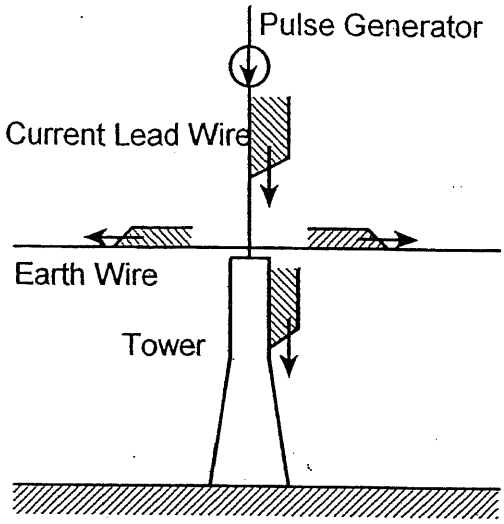

(b) Downward traveling current to a tower.

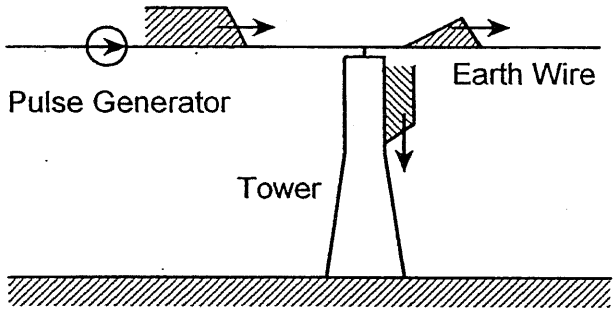

(c) Stroke to mid-span.

Fig. 3.9 Schematic diagrams for the measurement of the current splitting ratio between a tower and an earth wire.

The computed waveforms of the current splitting into the tower and into one side of the earth wire are shown in Fig. 3.10. In Figs. 3.10 (a) and (b), the injected current splits into the tower and into the earth wire at a fixed ratio until 0.8 μs, which is the arrival time of the reflected wave from the ground. In Fig. 3.10 (c), the current splitting into the tower increases gradually before 0.8 μs. This effect is ascribable to the induced current in the tower as was stated above.

Figure 3.11 shows time variations of the tower surge impedance evaluated from Fig. 3.10, assuming the impedance of the earth wire to be the surge impedance in the TEM mode (467 Ω). In the case of a return stroke to the tower, the surge impedance of the tower is about 250 Ω, and about 280 Ω in the case of a downward traveling current. These values are higher than

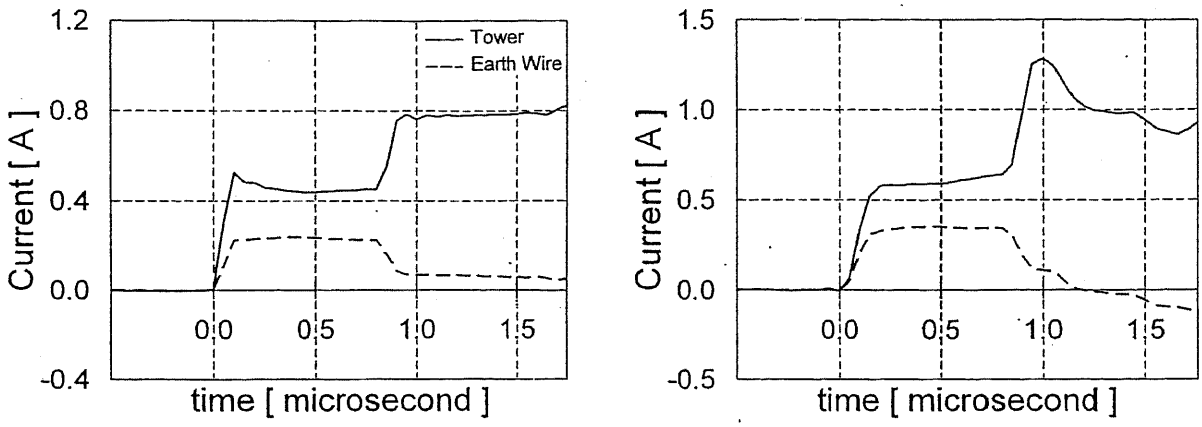

(a) Return stroke to the tower. (b) Downward traveling current to the tower.

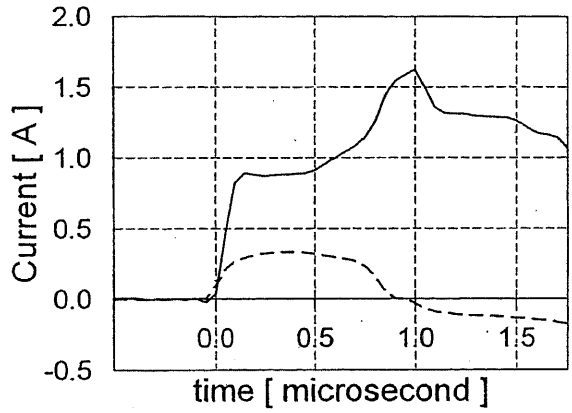

(c) Stroke to mid-span.

Fig. 3.10 Computed waveforms of the current splitting into the tower and an earth wire.

those evaluated by the direct method in Table 3.1 and Table 3.2 for more than 25 %. In the case of a stroke to mid-span, the tower surge impedance is about 180 Ω at 0.35 μs of its peak, which is about 10 % lower than that by the direct method. The tower surge impedance characterized by the refraction method of Fig. 3.10 (c) shows gradual decrease with time, which is due to the induced current in the tower.

The difference of the tower surge impedances dependent on the arrangement in the measurement can be explained by the electric field associated with the steep-front currents flowing in the current lead wire, the earth wire and the tower. In Fig. 3.12 (a), the currents flowing into both sides of the earth wire hardly produce the horizontal electric field in the vicinity of the connecting point since they have opposite directions, and the positive current flowing into the

tower and the negative current propagating up the vertical current lead wire produce the strong upward electric field. This makes the injected current split more into the earth wire and less into the tower than in the case of Fig. 3.12 (b), resulting in higher tower surge impedances.

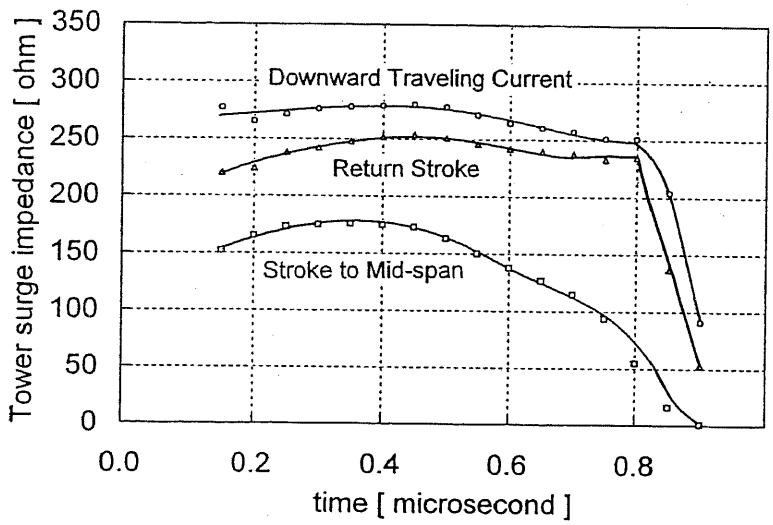

Fig. 3.11 Time variations of the tower surge impedance evaluated on the basis of the current splitting ratio at the the tower top.

Table 3.3 Tower surge impedances evaluated on the basis of the current splitting ratio at the tower top.

Type of lightning	Return stroke	Downward traveling current	Stroke to mid-span
Surge impedance	250 Ω	280 Ω	180 Ω

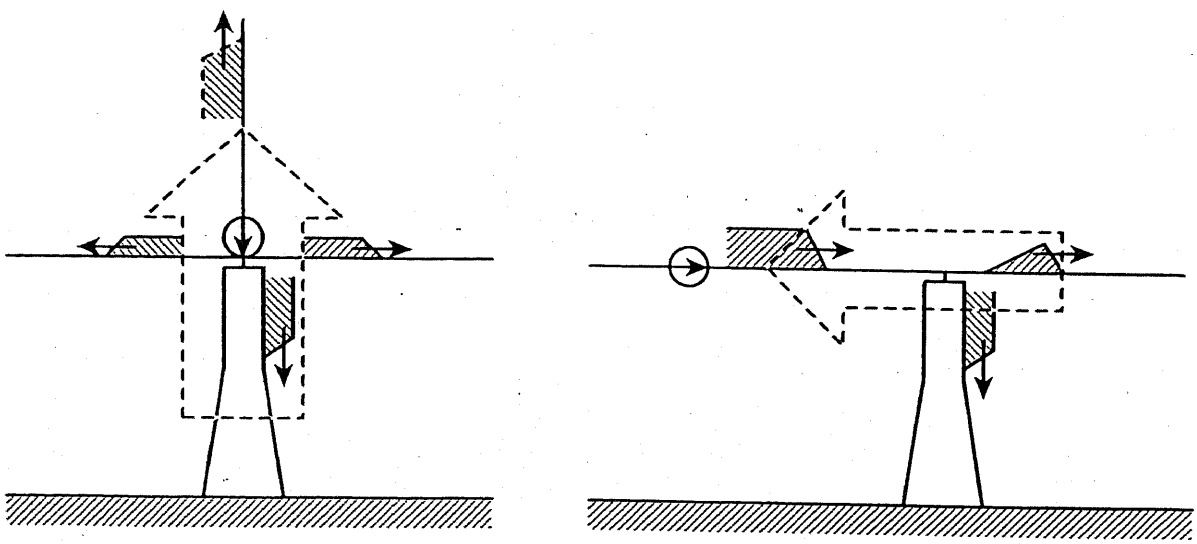

(a) Stroke to the tower. (b) Stroke to mid-span.

Fig. 3.12 Illustrative example of the dominant electric field around a tower system.

3.4 Estimation of the Surge Impedance of Double-Circuit Transmission Towers

Figure 3.13 illustrates 1000 kV and 500 kV double-circuit transmission towers, which are typical lattice towers in Japan. The surge impedances of these towers have been measured by the direct method. In the measurements, earth wires were disconnected. The tower of UHV I was measured in the vertical arrangement on a 100-to-1 reduced-scale model, and the surge impedance was 144 Ω [40]. The others are full-sized towers and were measured in different arrangements of the current lead wire. The surge impedances of these towers corrected to those for the vertical arrangement are summarized in Table 3.4, with the dimensions of the towers.

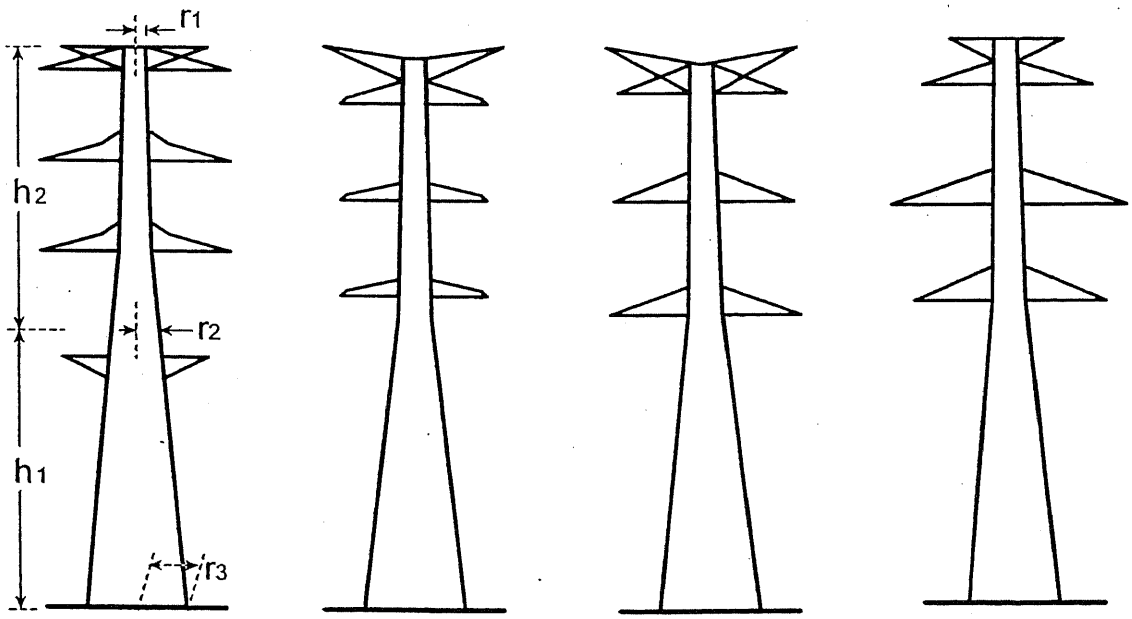

(a)UHV I. (b)UHV II. (c)500kV I. (d)500kV II.

Fig. 3.13 Structures of 1000kV and 500kV double-circuit towers.

Table 3.4 Surge impedances of various double-circuit towers measured by the direct method, and dimension of them.

Tower	UHV I [40]	UHV II [11]	500kV I [9]	500kV II [10]
Z_T (Ω)	144	*145	*148	*145
r_1 (m)	3.0	2.5	1.5	1.0
r_2 (m)	6.5	4.0	2.3	1.9
r_3 (m)	14	11	5.6	4.0
h_1 (m)	80	60	31	24
h_2 (m)	80	60	31	24

* corrected values

The dimensions of UHV I tower indicated in Table 3.4 are those of the original full-sized tower. The correction was made by using Fig. 3.6. In the case of UHV II tower, for example, the current lead wire and the voltage measuring wire were on a horizontal plane in the angle of 130°: it is known from Fig. 3.6 (a) that the measured surge impedance of 126 Ω [11] would be 134 Ω if the angle between the two wires were 90°: this value of 134 Ω corresponds to the condition of 0° in Fig. 3.6 (b), and is again corrected into the condition of 90°, i.e., vertical current injection, yielding 145 Ω.

It turned out that each of the towers had about the same impedance of 150 Ω as an independent tower, when it was measured by the direct method in the vertical arrangement.

Fisher *et al.* reported the surge impedance of a 345 kV double-circuit transmission tower to be 135 Ω [14] on the basis of the measurement in the vertical arrangement on a 25-to-1 reduced-scale model. The about 10 % difference from 150 Ω supposedly arose from the loading effect of 1 kΩ isolating resistors inserted at the input ends of the voltage measuring wires.

If the tower surge impedance of a typical double-circuit tower measured by the direct method in the vertical arrangement of the current injection wire is about 150 Ω, those characterized by the current splitting ratio at the top of the tower are estimated to be about 190 Ω for a vertical current injection and about 130 Ω for a horizontal one.

Chapter 4

Lightning Surge Response of Earth-Wired Tower

The apparent surge characteristics of a tower may be influenced by the presence of an earth wire, however, this issue has been paid little attention in the modeling of a tower for the EMTP simulations or in determining the parameters of a model. In this chapter, the surge characteristics of an earth-wired tower as well as a tower without earth wires struck by a vertical lightning stroke are studied with the help of NEC-2. Particularly, the transient behavior of the tower footing impedance, and that of the coupling coefficient between an earth wire and a phase conductor, which influences the voltage across an insulator, are investigated.

4.1 Numerical Electromagnetic Analysis of Earth-Wired Tower Struck by Lightning

4.1.1 Setup for Numerical Analysis

In the analysis, two kinds of lightning strokes are simulated: one is a return stroke, and the other is a downward traveling current wave, shown in Fig. 4.1.

In the case of a return stroke to a tower, a downward leader, which is similar to a charged vertical transmission line whose lower end is open, contacts the top of the tower. This situation can be simulated by placing a pulse current generator at the tower top, except for an actually slower velocity of return current wave than the velocity of light. Experiments on reduced-scale models [14][41], which employed a spiral wire or a straight wire suspended vertically above the tower, show that the speed of upward moving current produces only second-order effects on the surge characteristics of a tower. Therefore, the analysis employing a vertical straight wire as a current lead wire can properly evaluate tower surge characteristics.

On the other hand, many of the lightning strokes hitting towers on the coastal area of the Sea of Japan in winter begin with upward leaders from the towers [42], and many of the lightning current pulses are not produced by what are called return strokes [43]. In such kinds of strokes,

a current wave is thought to propagate down the lightning channel from the cloud to the tower top. For the simulation of this situation, a pulse current generator needs to be remotely placed above the channel. In the present analysis, a pulse current generator is inserted into the current lead wire at 240 m from the tower top, where the current lead wire is 480 m in length.

The arrangement for analysis is illustrated in Fig. 4.2. The model tower is the same as that of Fig. 3.4, which is composed of four main poles. Each pole is connected to the perfectly conducting plane through resistance of 40 Ω to realize the tower footing resistance of 10 Ω.

A horizontal earth wire is attached to the tower top at a height of 120 m, and phase conductors are stretched in parallel at a height of 108 m, 84 m and 60 m, respectively, at a distance of 10 m from the tower body. Each conductor or wire is 960 m in length and 0.1 m in radius. The ends of them are stretched down and connected to the ground through matching resistance. This terminating condition does not affect the phenomena at the tower within 3.2 μs.

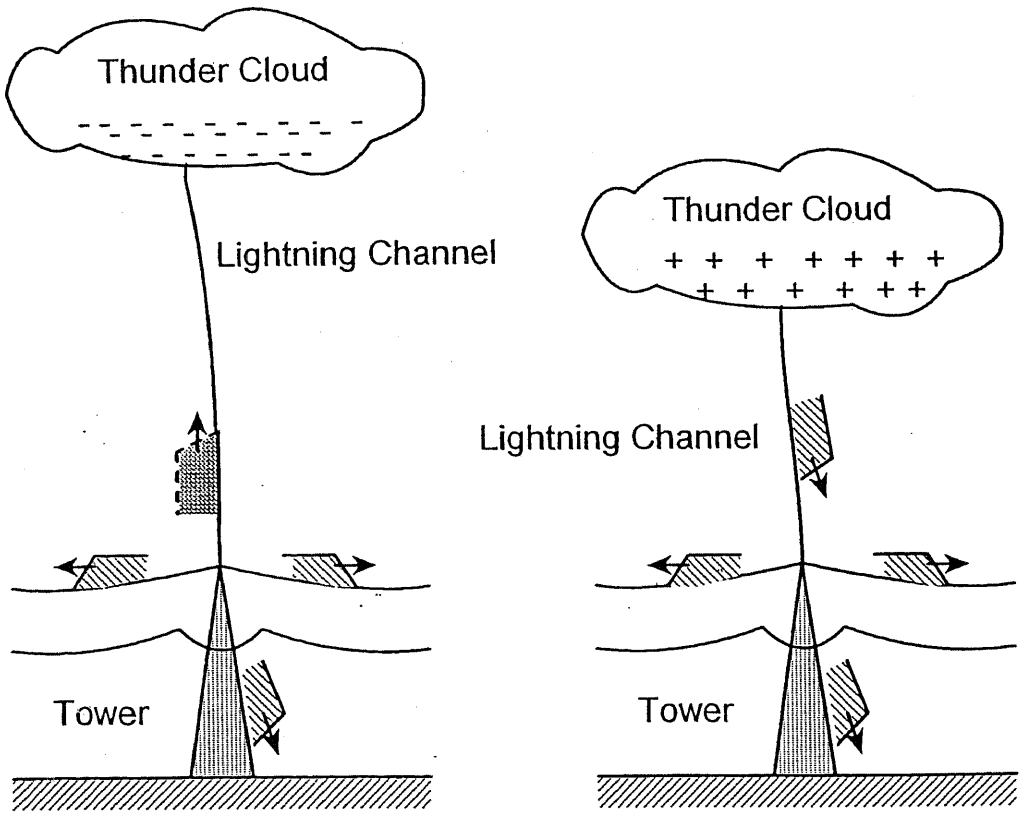

(a) Return stroke. (b) Downward traveling current wave.

Fig. 4.1 Schematic diagrams of different types of lightning strokes to the top of a tower.

An insulator voltage is evaluated through the current flowing a 100 kΩ resistive element inserted between the tower body and the phase conductor. In the same way, the voltage between a phase conductor and an auxiliary voltage measuring wire is evaluated. The horizontal auxiliary wire is stretched perpendicularly to the phase conductor. In this thesis, the voltage of crossarm is defined as the sum of an insulator voltage and a phase conductor voltage. To save the computation time, the phase conductor of interest only is equipped, and other phase conductors are removed.

For the numerical analysis, the conductors of the system are divided into 10 m or 12 m segments. The internal impedance of the pulse generator is 5 kΩ. Computation is carried out in the frequency range of 39.06 kHz to 20 MHz with the increment step of 39.06 kHz. This corresponds to the time range of 0 to 25.6 μs with 0.05 μs increments. The computation time with a Pentium 400 MHz processor with 64 MB RAM is about 15 minutes for the maximum case. A sample input data deck to NEC-2 for the analysis in the present chapter is shown in Appendix A.

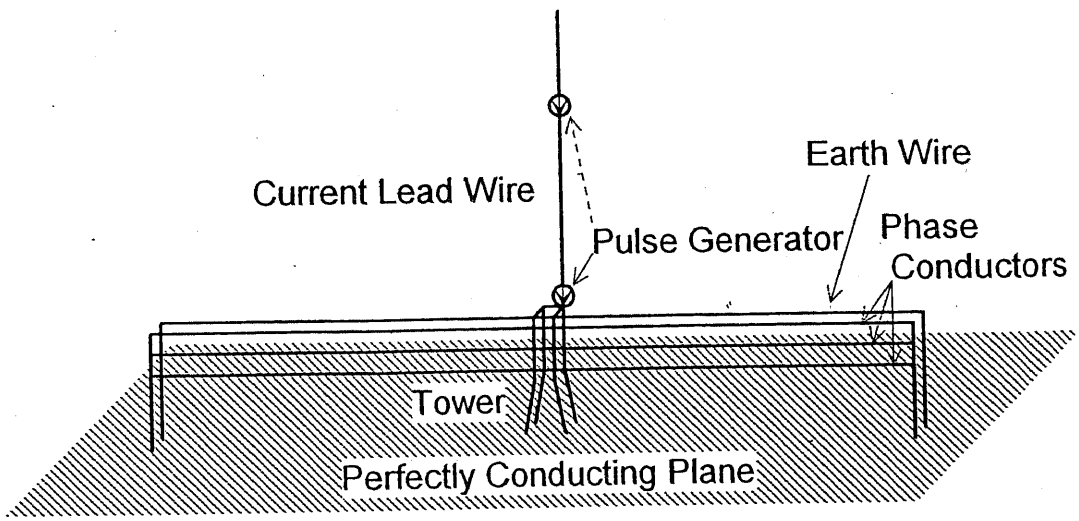

Fig. 4.2 Arrangement for the analysis simulating a vertical stroke hitting the top of a tower.

4.1.2 Step Response of Earth-Wired Tower

The computed waveforms of the currents splitting into the tower and an earth wire, and those of the voltages of various parts for the case of a return stroke are shown in Fig. 4.3. Those for the other case of current injection, a current wave traveling down the current lead wire, are shown in Fig. 4.4.

The transfer impedance of various parts of the tower is calculated so as to make quantitative evaluation. The transfer impedance, in this thesis, is defined as the ratio of the instantaneous value of the voltage to the current flowing into the tower at the moment of the peak of the insulator voltage. The calculated transfer impedances are summarized in Tables 4.1 and 4.2.

Tables 4.1 and 4.2 show that the transfer impedances are not much dependent on the mode of current injection. The transfer impedances of crossarms are hardly influenced by the presence of an earth wire. On the other hand, the transfer impedance for the insulator voltage is naturally much lower with an earth wire than that without an earth wire due to the coupling between the earth wire and a phase conductor.

Table 4.1 Transfer impedances of various parts of the tower for the case of return stroke. (Ω)

	Earth-wired				Independent			
	Top	U-phase	M-phase	L-phase	Top	U-phase	M-phase	L-phase
Crossarm	208	223	201	168	198	214	199	167
Insulator	—	176	178	159	—	224	197	168
Phase cond.	—	47	23	9	—	-7	-2	1

Table 4.2 Transfer impedances of various parts of the tower for the case of downward traveling current. (Ω)

	Earth-wired				Independent			
	Top	U-phase	M-phase	L-phase	Top	U-phase	M-phase	L-phase
Crossarm	215	225	208	181	207	222	206	178
Insulator	—	171	180	165	—	225	207	179
Phase cond.	—	54	28	16	—	-3	-1	1

Table 4.3 Computed coupling coefficient between the earth wire and a phase conductor at the moment of the peak of insulator voltage for different injection modes of step current.

	E.W. — U phase	E.W. — M phase	E.W. — L phase
TEM mode	0.345 – 100%	0.218 – 100%	0.140 – 100%
Return stroke	0.227 — 66%	0.110 — 50%	0.051 — 36%
Down. current	0.257 — 74%	0.133 — 61%	0.077 — 55%

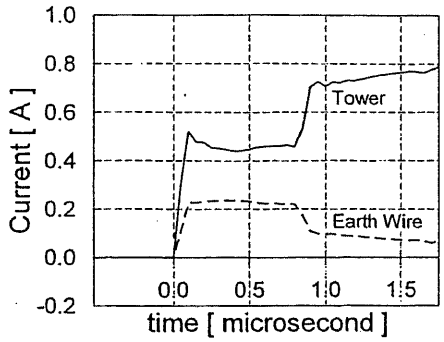

(a) Current into tower or earth wire.

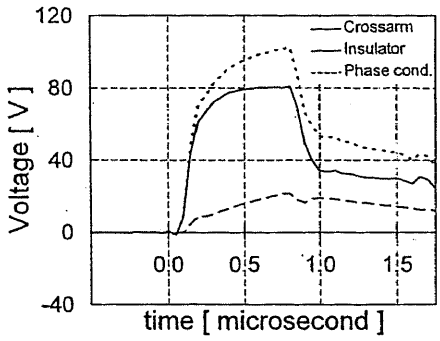

(b) Voltages on upper phase.

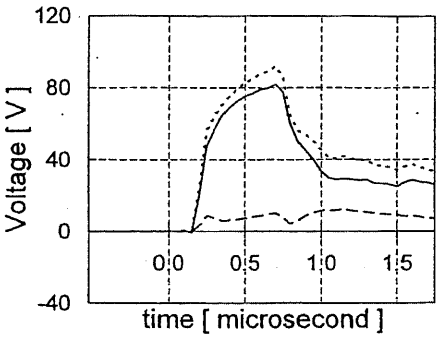

(c) Voltages on middle phase.

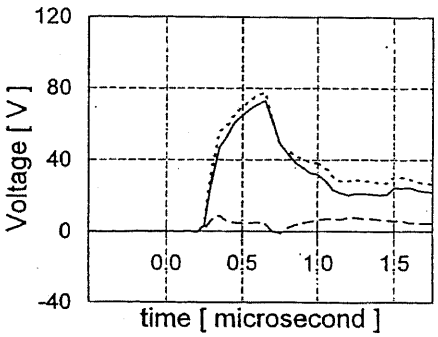

(c) Voltages on lower phase.

Fig. 4.3 Computed waveforms of currents and voltages in the system for the case of a return stroke to the tower top.

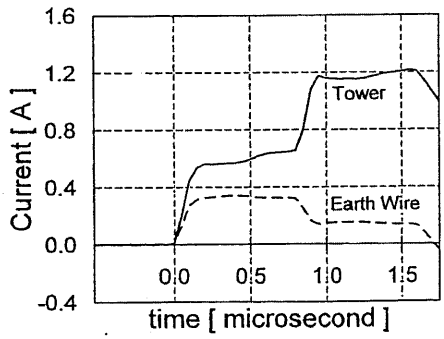

(a) Current into tower or earth wire.

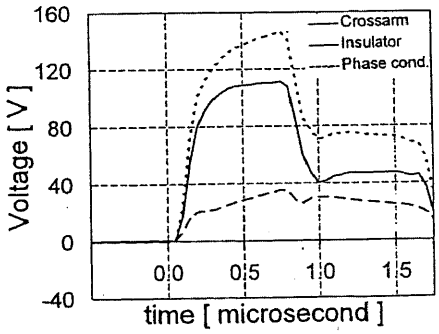

(b) Voltages on upper phase.

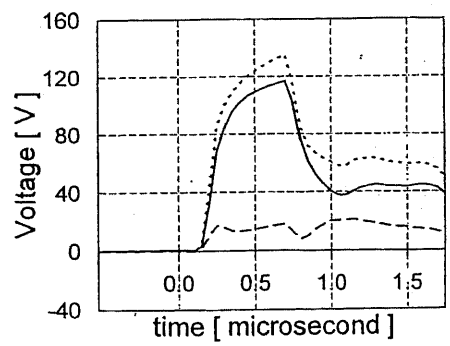

(c) Voltages on middle phase.

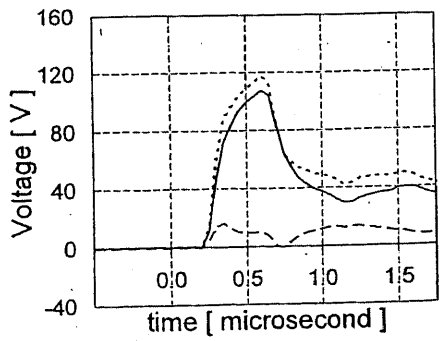

(c) Voltages on lower phase.

Fig. 4.4 Computed waveforms of currents and voltages in the system for the case of a downward traveling current to the tower top.

The coupling coefficient between the earth wire and a phase conductor, which is calculated at the moment of the peak of the relevant insulator voltage, is summarized in Table 4.3. The coupling coefficient is defined as the ratio of the voltage of the earth wire to that of a phase conductor, where the voltage of the earth wire is equal to that of the tower top. The coupling coefficients in the TEM mode or in the steady state, which are calculated through the following relation, are also shown in Table 4.3 as references.

$$k_{TEM} = \frac{\ln(b/a)}{\ln(2h/r)}, \tag{4.1}$$

where a is a distance between the earth wire and a phase conductor, b is a distance between the image of the earth wire and the phase conductor, r is the radius of the earth wire, and h is the height of the earth wire as illustrated in Fig. 4.5.

The coupling coefficient at the moment of the peak of the insulator voltage is much lower than that in the TEM mode. This phenomenon is studied further in chapter 4.3.

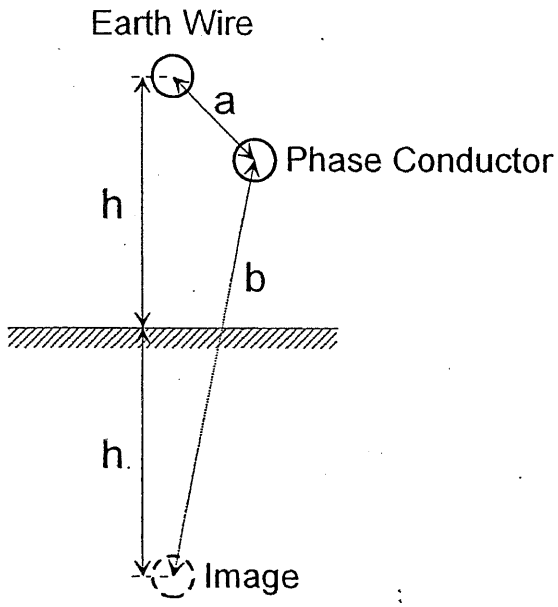

Fig. 4.5 Configuration of horizontal conductors.

4.1.3 Characterization of Tower Surge Response

The waveforms of crossarm voltages to the step current injection are characterized by the exponential rise and decay, which are physically ascribable to the initial electromagnetic field expanding spherically around the tower.

The voltage of the upper insulator rises steeply and then saturates, while the rate of rise of the middle or lower insulator voltage does less steeply. This is because the upper-phase conductor is more affected by the induction from the earth wire, whose voltage also rises exponentially.

At 1.6 μs, which is the time that the traveling wave makes two round trips in the tower, the transfer impedance of the upper crossarm is about 50 Ω and that of the lower crossarm is about 40 Ω. These are much higher than the footing resistance of 10 Ω. The differences do not mean the voltage drop along the tower, but they show that the electromagnetic field around the tower at the moment is still changing dynamically.

The injected current splits at a fixed ratio into the tower and into the earth wire from the beginning, because the impedance of the earth wire also rises exponentially until it reaches the value of the surge impedance.

4.2 Transient Tower Footing Impedance

If the impedance of the earth wire is assumed to be the surge impedance in the TEM mode ($Z_E = 467\Omega$) , the impedance of the model tower is estimated to be about 250 Ω ($= Z_E I_E / I_T$), as shown in Fig. 4.6, from the initial flat parts of the splitting currents shown in Fig. 4.3 (a). Figure 4.7 shows the comparison between the current splitting into the tower top computed by NEC-2 and that computed by EMTP. In the EMTP analysis, the tower is assumed as a lossless uniform transmission line having the surge impedance of 250 Ω, terminated by the footing resistance of 10 Ω, and the surge propagation velocity in this line is set equal to the speed of light. The suppressed tower current after the first reflection from the ground, computed by NEC-2, shows the presence of high footing impedance.

The transient impedance of the tower foot can be estimated more rigoriously from the reflected current wave shown in Fig. 4.3 (a) or in Fig. 4.7 in the same way as the Time-Domain Reflectometry (TDR). Figure 4.8 illustrates the assumed circuit of the tower system for the estimation of tower footing impedance, where the tower is regarded as the lossless line. The apparent tower footing imedance, Z_F, is calculated from the following relation:

$$\frac{I_{T2}}{I_{T1}} = 1 - \frac{Z_F - Z_T}{Z_T + Z_F} \cdot (1 - \frac{Z_{ES} - Z_T}{Z_T + Z_{ES}}), \tag{4.2}$$

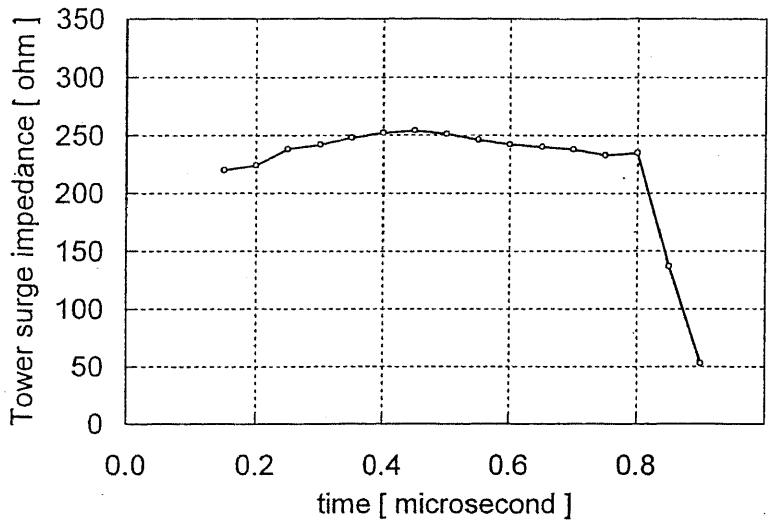

Fig. 4.6 Time variation of the tower surge impedance evaluated from the current splitting ratio at the tower top.

where I_{T1} is the magnitude of the step current splitting initially into a tower, I_{T2} is that of the tower current after the first reflection returns to the tower top from the ground, Z_T is the tower surge impedance, and Z_{ES} is the equivalent impedance representing the earth wire and the source seen from the tower.

The footing impedance initially exhibits about 75 Ω or even higher although the footing resistance is 10 Ω. This agrees with the result shown by Chisholm *et al.* [44], who identified the footing impedance of a conical tower on a perfectly conducting plane as 60 Ω by the TDR. At 1.6 μs, the footing impedance of the model tower evaluated from the reflected current falls off to about 55 Ω, which is almost the same as the transfer impedances of crossarms.

When the structure of a vertical conductor or four vertical conductors, whose base is directly connected to the perfectly conducting plane, is employed in place of the base-broadened model tower, the footing impedance is initially about 45 Ω and falls to about 25 Ω or 30 Ω at 1.6 μs for the case of single conductor or four conductors, respectively. These values are about 20 Ω lower than those of the base-broadened model tower. The employed single conductor is 120 m in height and 0.1 m in radius. The structure comprising four vertical conductors has the square cross section whose one side length is 10 m, and each conductor is 120 m in height and 0.1 m in radius. Figure 4.9 shows the current splitting into the top of the single vertical conductor computed by EMTP, assuming the conductor as a lossless uniform line having the surge impedance of 540 Ω, and that computed by NEC-2.

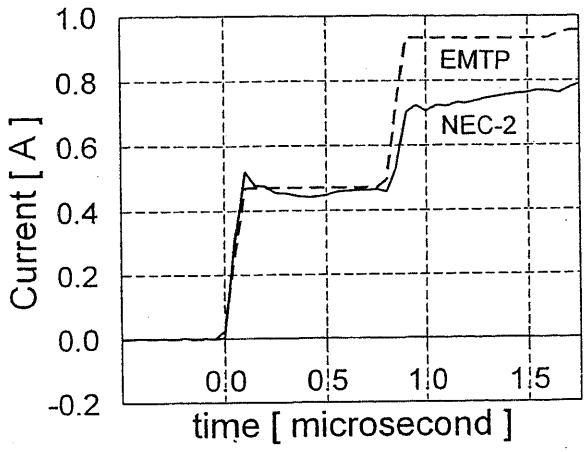

Fig. 4.7 The current splitting into the tower top computed by NEC-2, and that computed by EMTP assuming the tower as a lossless uniform line terminated by 10 Ω footing resistance.

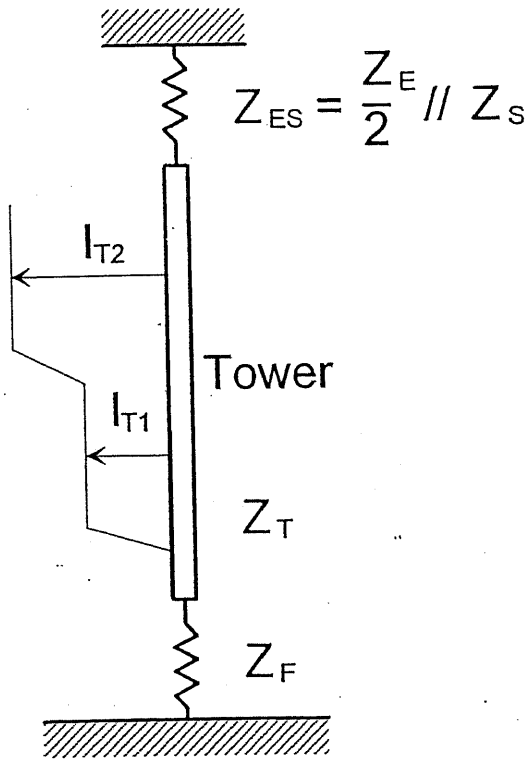

Fig. 4.8 Assumed circuit for the estimation of tower footing impedance.

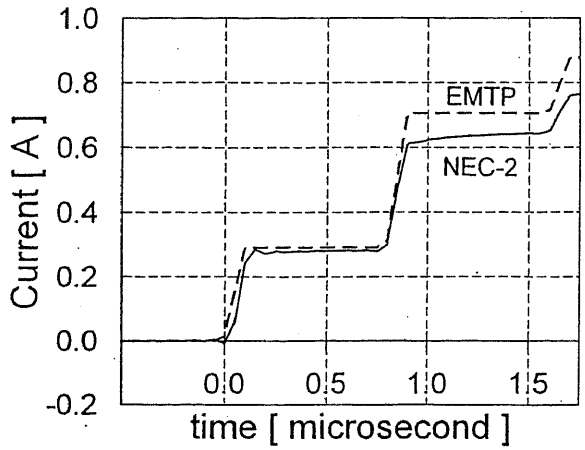

Fig. 4.9 The current splitting into the top of a single vertical conductor computed by NEC-2, and that computed by EMTP assuming the conductor as a lossless uniform line connected directly to the perfectly conducting plane.

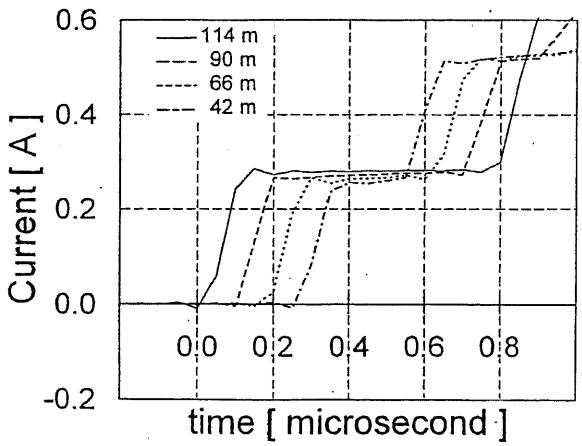

Fig. 4.10 Propagating current observed at a different height of a single vertical conductor.

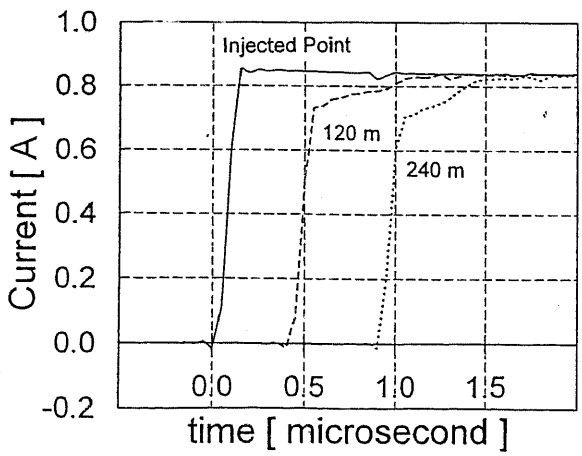

Fig. 4.11 Distortion of the propagating current on a horizontal conductor.
(length : 480 m, height : 120 m, radius : 0.1 m)

To clarify this phenomenon, the current propagating the single vertical conductor is computed at a different height in the same arrangement of Fig. 4.2. Figure 4.10 shows the waveforms of the current flowing into the vertical conductor observed at different heights. The current wave is reflected almost completely from the ground, however, it is distorted with its propagation. This wave-front distortion is probably attributable to the strong axial electric field associated with the fast-front propagating current itself. In the propagating current on a horizontal conductor, therefore, this wave-front distortion is also observed as shown in Fig. 4.11. The solid line expresses the current wave observed at the injected point of pulse current, the broken line does that observed at 120 m from the injected point, and the dotted line does that observed at 240 m from the injected point. The rectangular current wave is distorted only for the first 1 μs, which is roughly equal to the round-trip time of the electromagnetic wave between the horizontal conductor and the ground, where the height of the horizontal conductor is 120 m. Accordingly, the initially high footing impedance is partly due to the distortion of the rectangular current wave associated with the strong axial electric field. It should be noted that the mechanism of this wave-front distortion is highly related to the radiation of electromagnetic wave.

The about 20 Ω higher value of the footing impedance of the base-broadened model tower than that of single vertical conductor or multiple vertical conductors is probably ascribable to its base structure as shown by Kato *et al.* [33]. This indicates that the electromagnetic wave associated with the tower current may not smoothly propagate into the image of the tower in case of such discontinuous base structures, compared to vertical conductors. This non-homogeneity of a waveguide also contributes to the initially high footing impedance.

This initially high footing impedance of the base-broadened structure corresponds to the attenuation coefficient of about 0.8 for a transmission line representing a tower, which agrees well with the conventionally used values [7].

4.3 Coupling Coefficients under Lightning Hit

4.3.1 Transient Coupling Coefficients Influenced by Tower Current

The time variation of the coupling coefficient is shown in Fig. 4.12. Figure 4.12 (a) shows the time variations with respect to the step current, and Fig. 4.12 (b) shows those with respect to the ramp current having the rise time of 1.0 μs. These are computed results for the case of a return stroke.

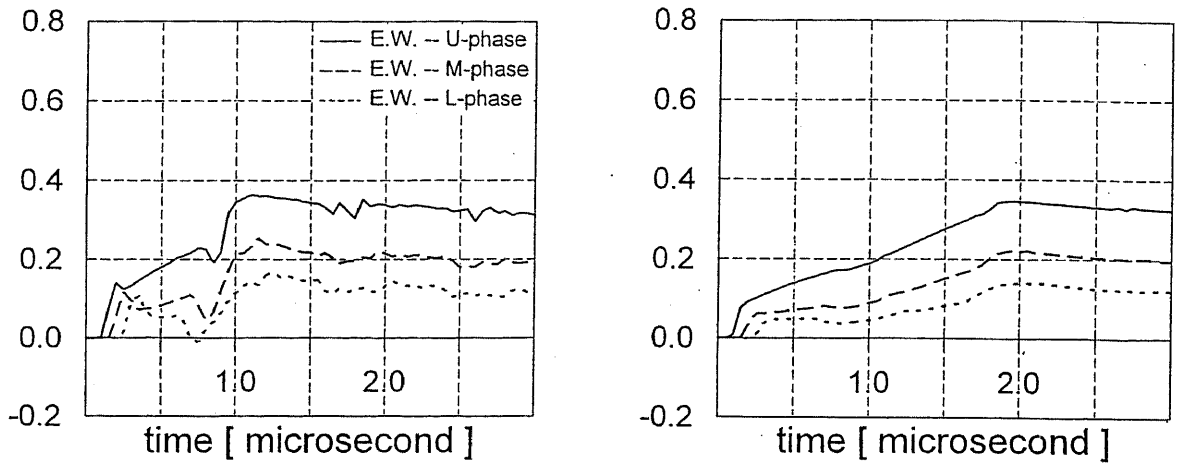

(a) Step current injection. (b) 1.0μs ramp current injection.

Fig. 4.12 Computed time variations of the coupling coefficient between the earth wire and a phase conductor.

Table 4.4 Computed coupling coefficient at the moment of the peak of insulator voltage for current of various waveforms. (TEM mode : 100%)

Rise time	E.W. - U phase	E.W. - M phase	E.W. - L phase
0.1 μs	66 %	50 %	36 %
1.0 μs	61 %	50 %	49 %
2.0 μs	73 %	66 %	64 %

The coupling coefficient at the moment of the peak of the insulator voltage is summarized in Table 4.4. It is much lower than the value in the TEM mode even for the current having a rise time of 2.0 μs. This initially low coupling coefficient is influenced by the transient upward electric field produced by the current wave in the tower, which cancels the downward field produced by the charge in the earth wire as shown in Fig. 4.13.

The coupling coefficients measured on an actual UHV transmission tower are compared with the values in the TEM mode in Table 4.5 [11]. The injected current was 1/70 μs triangular wave. The measured coupling coefficients in Table 4.5 are about 10 % still lower than those computed by NEC-2 in Table 4.4. The arrangement of the measuring wires in the experiment is the cause of this still lower coupling coefficient. In the experiment, the current propagating the horizontal current lead wire, which was stretched in extension of the voltage measuring wire, produced electric field suppressing the induced voltage between a phase conductor and the voltage measuring wire.

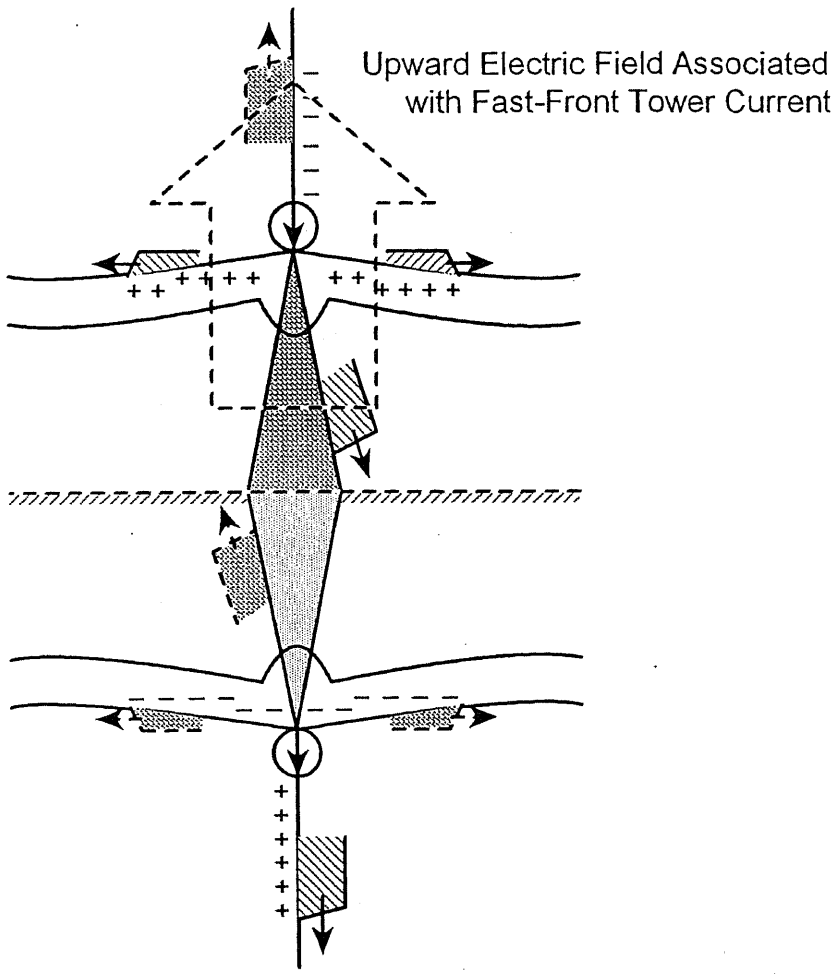

Fig. 4.13 Illustrative example of electric fields around a tower system.

Table 4.5 Measured coupling coefficient between the earth wires and a phase conductor of a UHV tower at the moment of the peak of insulator voltage for 1/70 μs current injection [11].

	E.W. - U phase	E.W. - M phase	E.W. - L phase
TEM mode	0.357 – 100 %	0.263 – 100 %	0.192 – 100 %
Measurement	0.161 — 45 %	0.099 — 38 %	0.079 — 41 %

The peak values of coupling coefficients in Fig. 4.12, which are computed by NEC-2, are summarized in Table 4.6 with their peak times. The coupling coefficient reaches its peak about 1 μs after the peak of the injected current. This delay of about 1 μs is roughly equal to the round-trip time of a traveling wave in the tower.

Table 4.6 Computed peak value and peak time of coupling coefficient for the current of various waveforms.

Rise time	E.W. - U phase	E.W. - M phase	E.W. - L phase
0.1 μs	105 % – 1.10 μs	117 % – 1.15 μs	119 % – 1.25 μs
1.0 μs	100 % – 1.95 μs	101 % – 1.95 μs	100 % – 2.00 μs
2.0 μs	99 % – 2.95 μs	98 % – 2.95 μs	94 % – 2.95 μs

4.3.2 Coupling Coefficients without Tower Current

The behavior of the coupling coefficient free from the influence of the tower current is investigated by computing its time variation with the use of NEC-2 in the arrangement like Fig. 4.2 without a tower. Figure 4.14 shows the result for the case of the step current injection. The coupling coefficient is apparently larger than the corresponding value of Table 4.3 at the moment of the peak of the insulator voltage. The influence of the tower current is obvious in the ragged waveforms of Fig. 4.12 (a) by comparing them with the smooth waveforms of Fig. 4.14.

The almost settled values of coupling coefficients in Fig. 4.14 are about 90 % of those in the TEM mode. The 10 % difference is probably caused by the negative charge in the vertical current lead wire, producing upward electric field around the current injection point.

To inspect this effect, the voltages of horizontal conductors are evaluated in the arrangement illustrated in Fig. 4.15, in which the effect of current lead wire on evaluated voltages or coupling coefficients is thought to be less. Figure 4.16 shows the computed time variation of the coupling coefficient. The settled values of coupling coefficients are about 95 % of those in the TEM mode. Therefore, the charge in the vertical current lead wire actually but slightly influences the coupling coefficients. It should be noted that the electric field in these cases settles to the TEM mode after the electromagnetic wave makes two round-trips between an earth wire and the ground [45], while the electric field in the arrangement of Fig. 4.2 including a tower does not settle so soon owing to the transient electric field associated with the current wave successively reflected at the ground and the tower top.

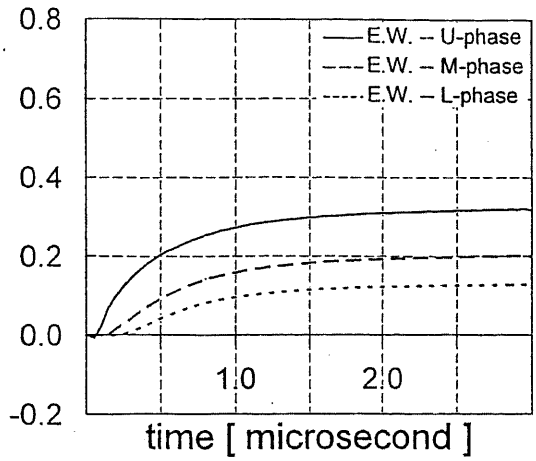

Fig. 4.14 Computed time variation of the coupling coefficient for the step current injection without a tower.

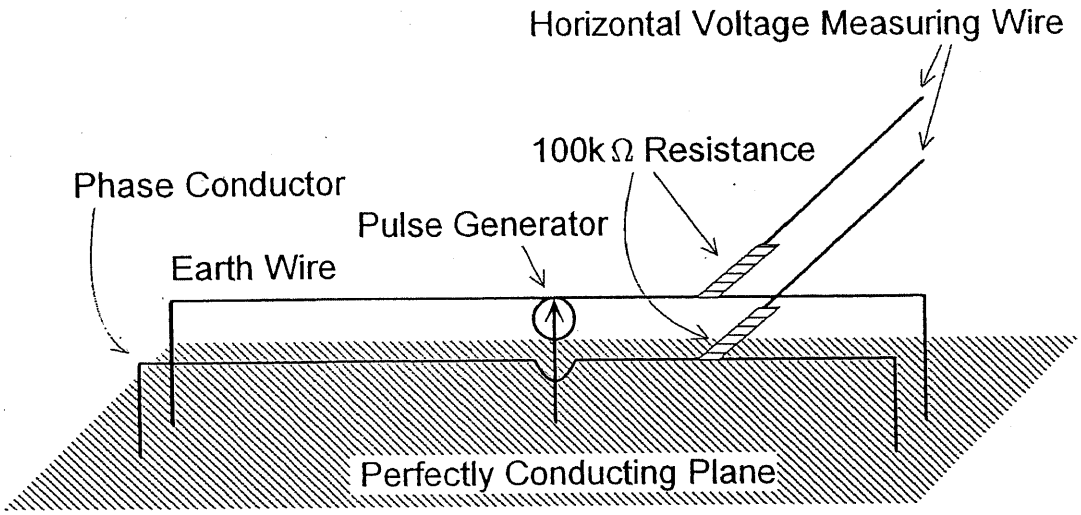

Fig. 4.15 Arrangement for the analysis employing a different method of current injection.

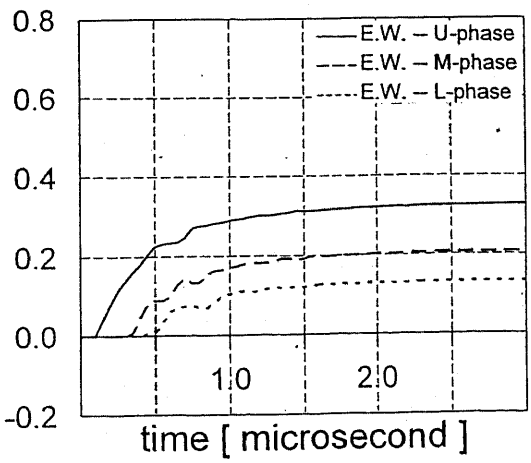

Fig. 4.16 Time variation of the coupling coefficient for the step current injection, computed for the arrangement of Fig. 4.15.

Chapter 5

Tower Models for EMTP Analysis

NEC-2 cannot exactly model the structures of actual towers, and in addition it cannot directly be interfaced with EMTP. For the EMTP simulations, therefore, it is practical to employ an equivalent circuit of the transmission-line type for the representation of a tower. In developing a tower model or in determining its parameters, characteristics stated in the preceding chapter should be taken into consideration. In this chapter, tower models proposed so far are reviewed with emphasis on their performance in reproduction of measured waveforms of insulator voltages. Then, a new procedure to determine the parameters of the multistory tower model for EMTP multi-conductor analyses on the basis of the measured insulator voltages is proposed.

5.1 Review on Tower Models for EMTP Simulations

5.1.1 Lossless Line Model

This model represents a tower by a lossless uniform transmission line having the length of the tower height. Although this simple representation may be suitable for the simplified estimation of lightning back-flashover probabilities [5], it cannot reproduce the complex waveforms of insulator voltages.

5.1.2 Distortionless Line Model

This model represents a tower by a uniform transmission line having constant attenuation. The representation by the surge impedance $Z_T = 100\ \Omega$, the surge propagation velocity in the tower $v = 0.7$ c, and the surge attenuation coefficient $\gamma = 0.7$ [4], which has been used in the estimation of lightning performance of transmission lines in Japan, is included in this category. The constant attenuation coefficient results in a high residual tower voltage as time elapses, so that the wave tail of the reproduced tower voltage deviates from the actual value.

5.1.3 Model Composed of Many Lossless Lines

This model is composed of many short lossless lines that represent vertical elements, slant elements and crossarms as illustrated in Fig. 5.1 [46]. The surge impedance of each part is determined from their dimensions and geometry, which is based on a series of experiments on reduced-scale models of independent towers.

The surge impedance of each line representing vertical elements, Z_{T1}, Z_{T2}, Z_{T3} and Z_{T4}, is given by

$$Z_{Tk} = 60\,(\ln \frac{2\sqrt{2}h_k}{r_{ek}} - 2), \qquad (k = 1, 2, 3, 4.) \tag{5.1}$$

where

$$r_{ek} = 2^{1/8}(r_{Tk}^{1/3} r_B^{2/3})^{1/4}(R_{Tk}^{1/3} R_B^{2/3})^{3/4}, \qquad (k = 1, 2, 3, 4.)$$

in which h_k, r_{Tk}, R_{Tk}, r_B and R_B are the lengths of the corresponding parts indicated in Fig. 5.1.

The surge impedance of each line representing slant elements, Z_{L1}, Z_{L2}, Z_{L3} and Z_{L4}, is given by

$$Z_{Lk} = 9Z_{Tk}. \qquad (k = 1, 2, 3, 4.) \tag{5.2}$$

The travel time in these lines is 1.5 times of those representing vertical elements.

The surge impedance of each line representing crossarms, Z_{A1}, Z_{A2}, Z_{A3} and Z_{A4}, is given by

$$Z_{Ak} = 60\,ln\frac{2h_k}{r_{Ak}}, \qquad (k = 1, 2, 3, 4.) \tag{5.3}$$

where h_k and r_{Ak} are the height and the equivalent radius of k-th crossarm, respectively. The length of each line of the crossarm is set equal to the actual arm length. The equivalent radius is chosen as 1/4 of the width of the arm at the junction point.

The measured and computed waveforms of the voltages of crossarms of an independent double-circuit transmission tower are shown in Fig. 5.2. The surge propagation velocity in these lines is equal to the speed of light. The computed waveforms agree well with the measured ones. In case this tower model is employed in the EMTP simulation of an earth-wired system, however, equation (5.1) will need modification to cope with the initially low coupling coefficient.

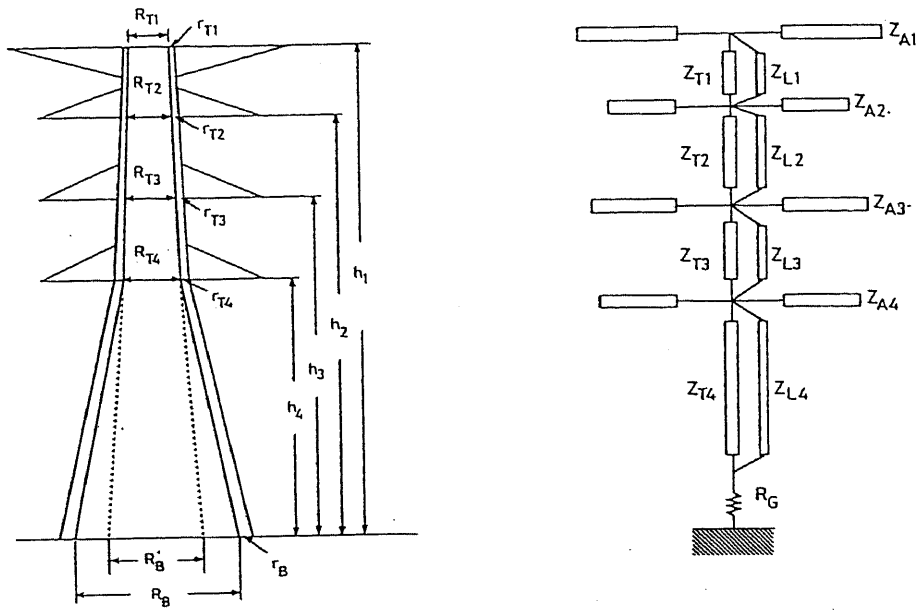

Fig. 5.1 Tower model proposed by Hara *et al.* [46].

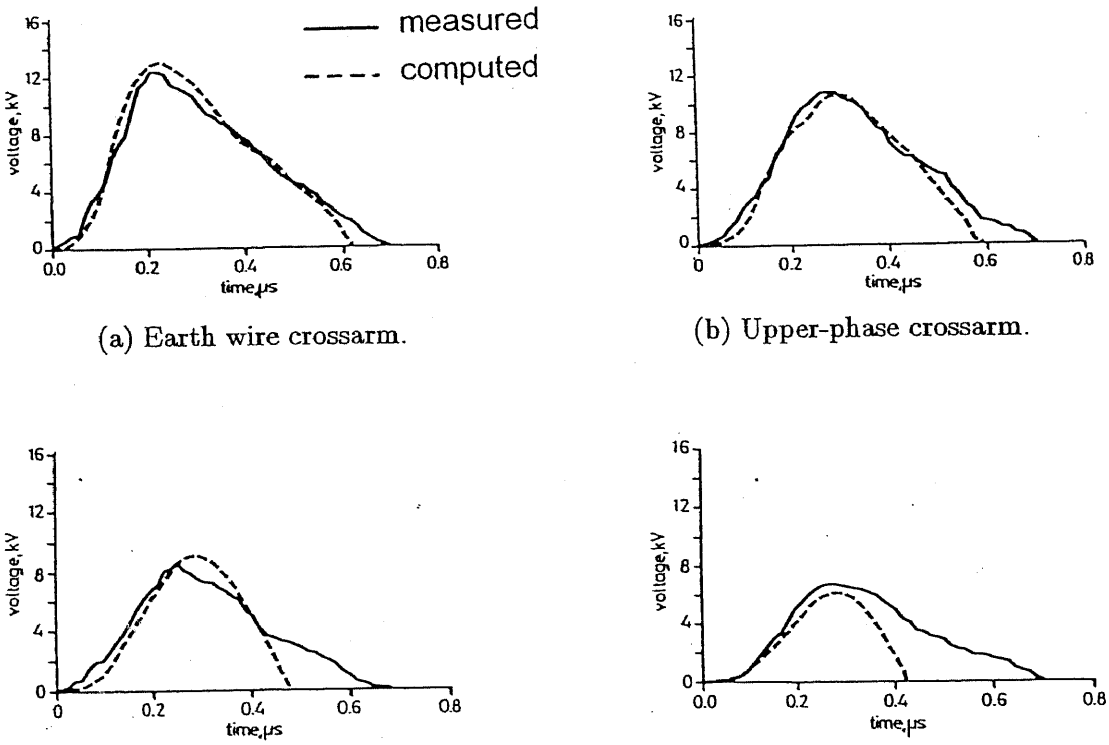

(a) Earth wire crossarm.

(b) Upper-phase crossarm.

(c) Middle-phase crossarm.

(d) Lower-phase crossarm.

Fig. 5.2 Measured and Computed waveforms of the crossarm voltages of an independent tower for the step current injection [46].

5.1.4 Multistory Tower Model

This tower model is composed of four sections divided at the upper, middle and lower phase crossarm positions. Each section consists of a lossless transmission line and a R - L parallel element as illustrated in Fig. 5.3 [9]. The resistance represents attenuation of traveling waves in the tower, and the inductance in parallel makes the resistance ineffective as time elapses, which enable good approximation of the waveforms of insulator voltages, including the wave tails.

The computed waveforms of insulator voltages, with the measured ones on a 500 kV double-circuit tower equipped with earth wires, are shown in Fig. 5.4. The computed waveforms agree well with the measured ones.

This model can easily be interfaced with EMTP, and is suitable for multi-conductor analyses. Table 5.1 summarizes different sets of the parameters of this model proposed so far. The values in [9] or [11] were determined by the measurements on an earth-wired 500 kV or UHV double-circuit tower. Those of [25] were based on the measurements on an earth-wired 275 kV double-circuit tower struck by natural lightning. Although the values of parameters need further investigation, the multistory model itself can cope with various results of measurements.

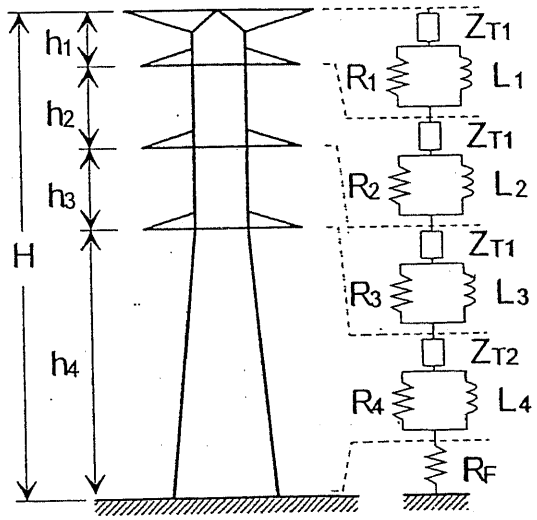

Fig. 5.3 Multistory model for a double-circuit tower [9].

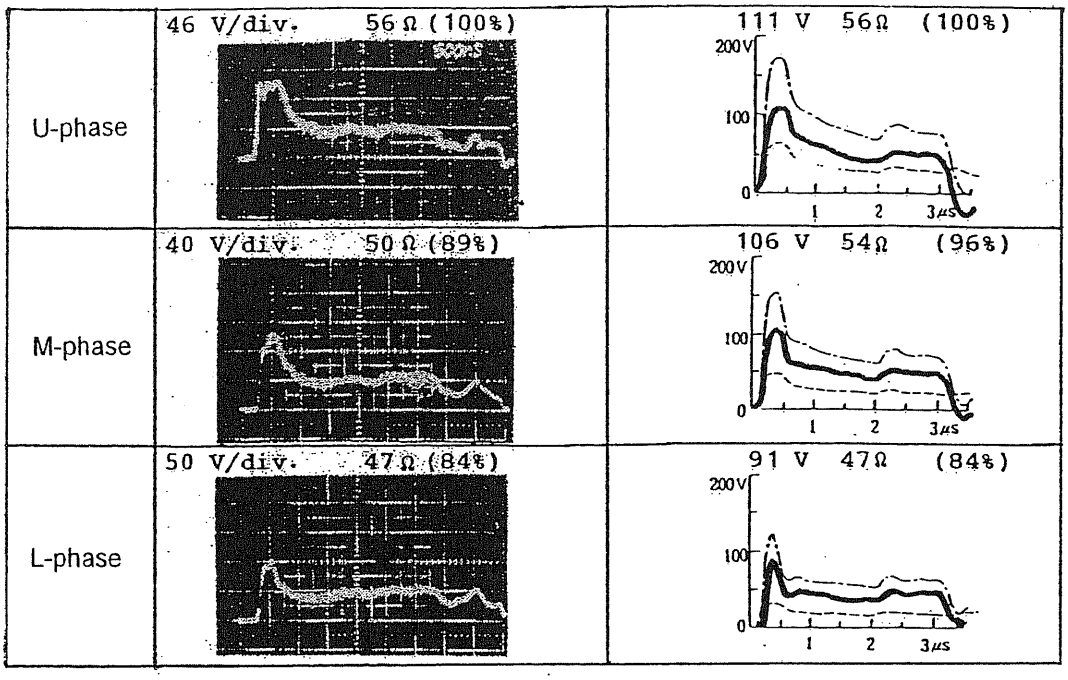

Fig. 5.4 Measured and computed waveforms of insulator voltages of an earth-wired 500kV double-circuit tower for the step current injection [9].

Table 5.1 Determined parameters for multistory tower model.

ref.	$Z_{T1}(\Omega)$	$Z_{T2}(\Omega)$	$v(\mathrm{m}/\mu\mathrm{s})$	γ	τ
[9]	220	150	300	0.8	2h/c
[11]	120	120	300	0.7	2h/c
[25]	120	120	300	0.8	2h/c

5.1.5 Nonuniform Line Models

This model represents a tower by a nonuniform transmission line [47]-[50] to express the distortion of a traveling wave. Oufi *et al.* [47] represented a tower by six- or three-story lossless lines whose surge impedance varies exponentially with location. Although an analytical solution in the frequency domain can be obtained for the voltage and current at any point along an exponential line, it is difficult to be interfaced with EMTP.

Almeida *et al.* [48] represented a tower by a lossless line with the surge impedance varying by discrete steps with location. The ratio of the surge impedance, from one segment of the line to the adjacent one, is assumed to be a constant. The waveforms of insulator voltages computed

to reproduce the measured waveforms of a 500 kV tower (Fig. 5.4) are shown in Fig. 5.5 (a). In the simulation, the tower was divided into 314 segments. The employed tower surge impedances are 220 Ω for the top of the model and 150 Ω for the bottom. The peak value of the computed lower-phase insulator voltage is the highest and that of upper-phase is the lowest, which is contradictory to the measured results as are shown in Fig. 5.4.

Barros *et al.* [49] represented a tower by a nonuniform line including frequency-independent loss. The surge impedance Z_T and the resistance per unit length R at the height of h are given by the following formulas:

$$Z_T(h) = k_1 + k_2\sqrt{h}, \tag{5.4}$$

$$R(h) = -2\frac{ln\sqrt{\gamma}}{H}Z_T(h), \tag{5.5}$$

where k_1 and k_2 are constants, γ is the attenuation coefficient, and H is the tower height. In the EMTP simulation, $k_1 = 150\ \Omega$, $k_2 = 8.83\ \Omega m^{-1/2}$, and $\gamma = 0.8$ were employed to simulate the measurement [9], and the result is shown in Fig. 5.5 (b). The peak value of the computed lower-phase insulator voltage is the highest and that of upper-phase is the lowest, which is contradictory to the measured results as are shown in Fig. 5.4.

Nguyen *et al.* [50] reduced the exponential line model proposed by Oufi *et al.* [47] to a form similar to that of Bergeron's method [51] as is illustrated in Fig. 5.6. Thus, this model is interfaced with EMTP. The computed insulator voltages agree with the corresponding measured ones [9] except for the residual tower voltage seen in Fig. 5.5 (c). In the simulation, capacitance of insulator strings and that between the phase conductors and the tower are postulated.

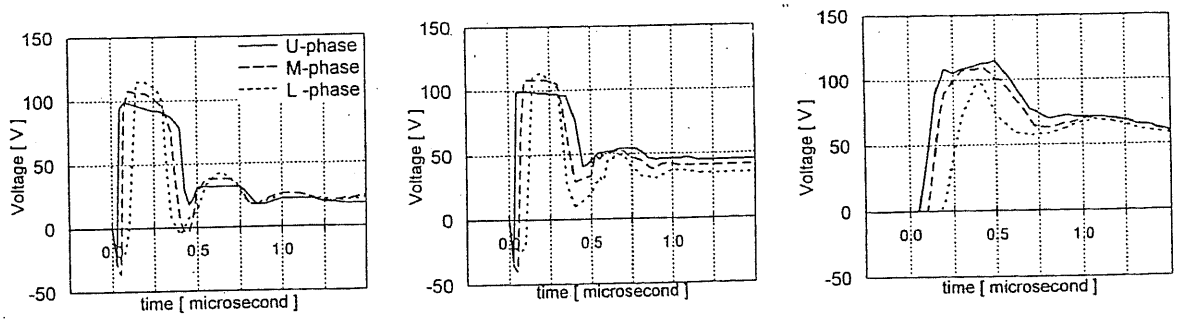

(a) Almeida *et al.*'s model [48]. (b) Barros *et al.*'s model [49]. (c) Nguyen *et al.*'s model [50].

Fig. 5.5 Waveforms of insulator voltages reproduced by nonuniform line models.

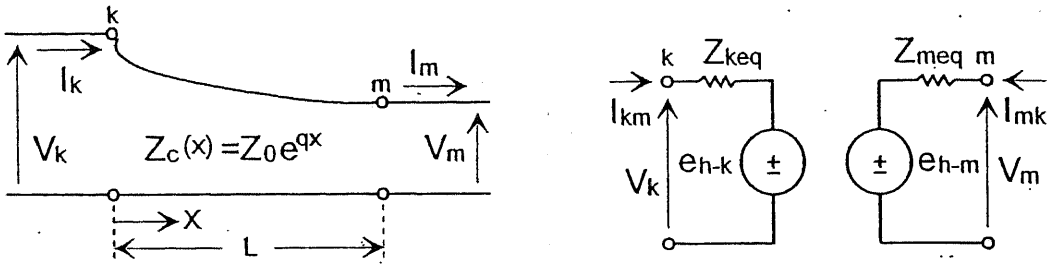

Fig. 5.6 Exponential line and its equivalent circuit [50].

5.1.6 Frequency-Dependent Line Models

This model represents a tower by a frequency-dependent line [52][53] to simulate distortion of traveling waves.

Nagaoka [52] represented a tower by a uniform line having a constant surge impedance and a frequency-dependent propagation constant, and they are determined from the step response of the tower top voltage. The surge impedance is determined from its initial value. The propagation constant in the frequency domain is determined from its decaying part, which is approximated by an exponential time function. This model can be interfaced with EMTP.

Kato *et al.* [53] represented a tower by a uniform line having frequency-dependent surge impedance and propagation constant. This model can reproduce the gradual rise of the step response of the tower top voltage of an independent tower in its initial part. The surge impedance Z_T and the propagation constant $\alpha + j\beta$ of this uniform line are expressed by the following formulas in the frequency domain:

$$Z_T(s) = \frac{Z_d}{\{1 + (sT_0)^m\}^n}, \tag{5.6}$$

$$\alpha H = 10^{(-k_1 + k_2 log|s|)}, \quad \beta = \frac{k_3 \omega H}{c},$$

where c is the velocity of light, H is the tower height, and T_0 is equal to $4h/c$.

The constants in the above equations, Z_d, m, n, k_1, k_2 and k_3, are determined from the step response of the tower top voltage of a tower.

Figure 5.7 (a) shows the step response of the tower top voltage of an independent tower computed by a numerical electromagnetic analysis [33]. Figure 5.7 (b) shows a waveform computed by this model for $Z_d = 168\ \Omega$, $m = 0.6$, $n = 1/2.4$, $k_1 = 1.5$, $k_2 = 0.5$ and $k_3 = 1.1$. Equation (5.6) needs to be expressed by a rational function to be interfaced with EMTP.

If the surge impedance of a tower in high frequencies is low so as to simulate the gradual rise of the tower top voltage like this model, it results in larger splitting current into the tower than in the actual case at the initial part of the waveform. For this reason, the reproduction of the initial rising part with maintaining the correct current-splitting ratio is essentially difficult for an earth-wired system. This part is, however, not important except for such an extremely fast-front lightning current whose rise time is much less than $2h/c$.

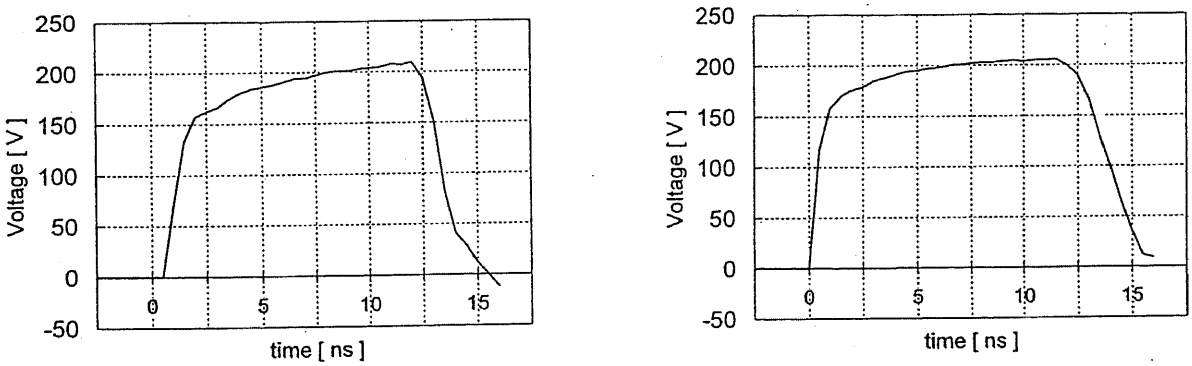

(a) Numerical electromagnetic analysis. (b) Frequency-dependent line model.

Fig. 5.7 Step-response waveforms of tower top voltage of an independent tower [53].

5.2 Parameters of Multistory Model for Earth-Wired System

The reviewed tower models are engineering models, and the parameters in the tower models need to be determined on the basis of the measured or exactly computed step-response waveforms. Among the engineering models, the multistory tower model is the simplest and the easiest to be understood. In determining its parameters, the step-response characteristics stated in chapter 4 should be taken into account.

(i) Initially low coupling coefficients.

(ii) Exponentially rising and decaying insulator voltages.

(iii) The initially high and gradually decaying footing impedance.

In the present chapter, a procedure to determine the parameters of the multistory tower model for an earth-wired tower is proposed.

In the lightning surge analysis of overhead transmission lines, it is highly important to reproduce the measured waveforms of insulator voltages as closely as possible, since insulator voltages directly determine the back-flashovers. For the reproduction of insulator voltages to the step current injection, the initially low coupling coefficient needs to be handled properly to be coupled with EMTP multi-phase line models, in which the TEM mode is postulated. It can be realized by increasing the surge impedance of a tower model to compensate the suppressed coupling coefficient, that is, the tower surge impedance Z_T is determined from the transfer impedance for the insulator voltage of upper phase $V_{U.INS}$ and the coupling coefficient between the earth wire and the upper-phase conductor in the TEM mode $k_{U.TEM}$ by the following relation:

$$Z_T = \frac{V_{U.INS}}{1 - k_{U.TEM}}. \tag{5.7}$$

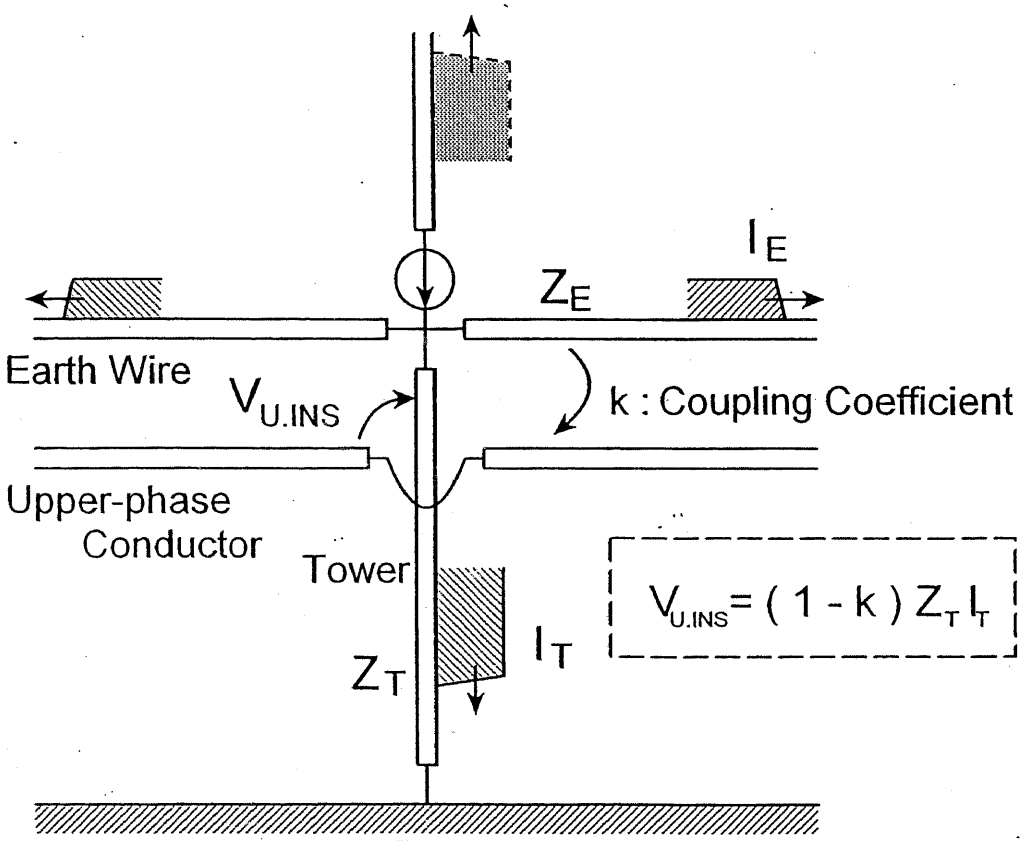

Fig. 5.8 Schematic diagram of the effect of tower surge impedance and coupling coefficient on the insulator voltage in the traveling wave analysis.

For the model tower with an earth wire employed in the present study, $Z_T = 270\Omega$ is determined from $V_{U.INS} = 176\Omega$ in Table 4.1 and $k_{U.TEM} = 0.345$ found in Table 4.3. This value is 35 % higher than the surge impedance of the same tower with no earth wires (200 Ω), however, it is favorably closer to the value representing the current-splitting ratio between the tower and the earth wire (250 Ω).

Figure 5.9 (a) shows the waveforms of insulator voltages computed by EMTP [54] when the tower is represented by the lossless uniform line having the surge impedance of 270 Ω. Although the peak value of the voltage of upper-phase insulator agrees with that computed by NEC-2 shown in Fig. 4.3 (b), those of the other phases much differ from the actual values.

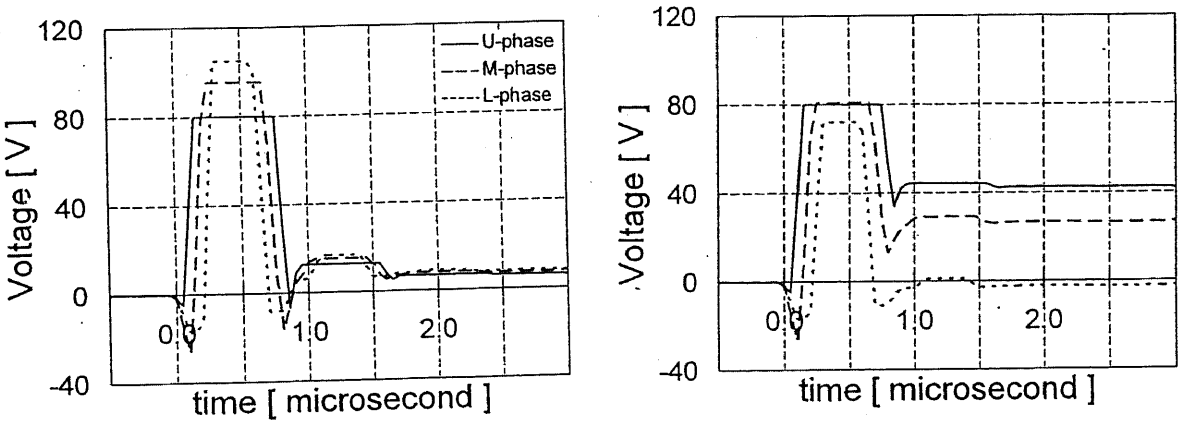

(a) Lossless line model. (b) Distortionless line model.

Fig. 5.9 Waveforms of insulator voltages computed by EMTP with simple tower models.

When the tower is represented by the distortionless line divided at crossarm positions as is illustrated in Fig. 5.10 (a), the attenuation coefficients γ_2 and γ_3 need to fulfill the following relations so as to reproduce the peaks of middle- and lower-phase insulator voltages, where Z_T is assumed to be 270 Ω and γ_1 is to be 1.0.

$$V_{M.INS} = Z_T(\gamma_2\gamma_1 - k_{M.TEM}) \tag{5.8}$$

$$V_{L.INS} = Z_T(\gamma_3\gamma_2\gamma_1 - k_{L.TEM}) \tag{5.9}$$

where $V_{M.INS}$ and $V_{L.INS}$ are insulator voltages of the middle and the lower phase in terms of transfer impedance, and $k_{M.TEM}$ and $k_{L.TEM}$ are coupling coefficients in the TEM mode of relevant phases.

From $V_{M.INS} = 178\Omega$, $V_{L.INS} = 159\Omega$ in Table 4.1, $k_{M.TEM} = 0.218$, and $k_{L.TEM} = 0.140$ in Table 4.3, $\gamma_2 = 0.88$ and $\gamma_3 = 0.83$ are determined. Figure 5.9 (b) shows the waveforms of insulator voltages computed by EMTP with this model. Although the peak values of each insulator voltage agree with that computed by NEC-2, the wave tails deviate from the actual cases.

When the equivalent circuit composed of lossless lines and lumped resistance illustrated in Fig. 5.10 (b) is employed in place of the circuit of Fig. 5.10 (a), Z_{T3}, Z_{T4}, R_2 and R_3 need to be determined so that the downward current wave may not be reflected at the nodes of the middle and the lower phase. From this condition, these four parameters are determined from the following four equations:

$$Z_{T2} = R_2 + Z_{T3}, \qquad \frac{2Z_{T3}}{(Z_{T2} + R_2) + Z_{T3}} = \gamma_2. \tag{5.10}$$

$$Z_{T3} = R_3 + Z_{T4}, \qquad \frac{2Z_{T4}}{(Z_{T3} + R_3) + Z_{T4}} = \gamma_3. \tag{5.11}$$

The exponential rise of the insulator voltage is essentially difficult to be simulated through an equivalent circuit for an earth-wired tower system as was stated in chapter 5.1.6. On the other hand, the exponentially decaying part can be reproduced by R-L parallel elements inserted in series. The decaying part is characterized by the steep decay right after the peak followed by a less-steep part. To represent this characteristic in the model, two R-L parallel elements in series, having different time constants, are inserted into the bottom section as illustrated in Fig. 5.10 (c). The values of R_4 and L_4 are determined taking account of the transient footing impedance at the moment of 1.6 μs. The initial high footing impedance and rapid decays are represented by R_5 and L_5. The time constants of the 2nd and 3rd story are set to τ, which is the round-trip time of a traveling wave in the tower (0.8 μs).

The determined parameters are listed in Table 5.2. These values are for the model tower, which is employed in the present analysis, having higher surge impedance than that of typical double-circuit towers. The estimated parameters for a typical double-circuit tower, taking account of the lower surge impedance than the model tower including no slant elements, are shown in parentheses in Table 5.2. They are obtained as follows: the value of 270 Ω of the model tower calculated by the above procedure is 35 % higher than the surge impedance of the same tower with no earth wires, and that of typical double-circuit towers without earth wires

is about 150 Ω, therefore, the value for typical towers based on insulator voltages is estimated to be about 200 Ω ($\simeq 150\Omega \times 1.35$).

The waveforms of insulator voltages computed by EMTP are shown in Fig. 5.11, with those computed by NEC-2. In the EMTP simulation, the surge propagation velocity in the tower is set equal to that of light (300 m/μs). The waveforms computed by EMTP agree well with those computed by NEC-2, also in the wave tails. The current-splitting ratio between the tower and the earth wire shown in Fig. 5.12 is well reproduced, too.

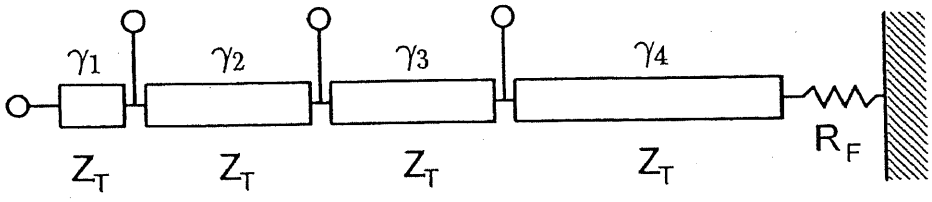

(a) Distortionless line model.

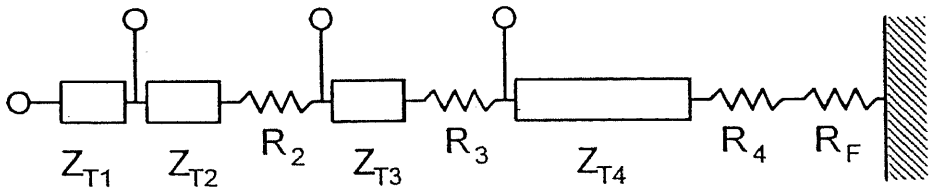

(b) Cascade line model composed of lossless lines and R elments.

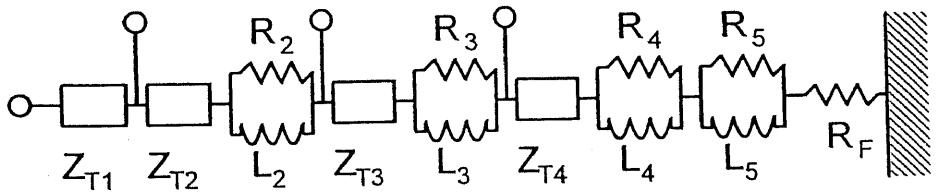

(c) Multistory tower model.

Fig. 5.10 Equivalent circuits for a tower.

Table 5.2 Parameters of the multistory tower model determined for the model tower employed in the present analysis.

Story	Surge impedance	Resistance	Time constant
1st	270 Ω (200 Ω)	0 Ω (0Ω)	—
2nd	270 Ω (200 Ω)	30 Ω (20 Ω)	τ
3rd	240 Ω (180 Ω)	40 Ω (30 Ω)	τ
4th	200 Ω (150 Ω)	35 Ω (25 Ω)	2τ
	——	35 Ω (25 Ω)	$0.2\,\tau$

* values in parentheses are for an actual double-circuit tower with crossarms and slant elements.

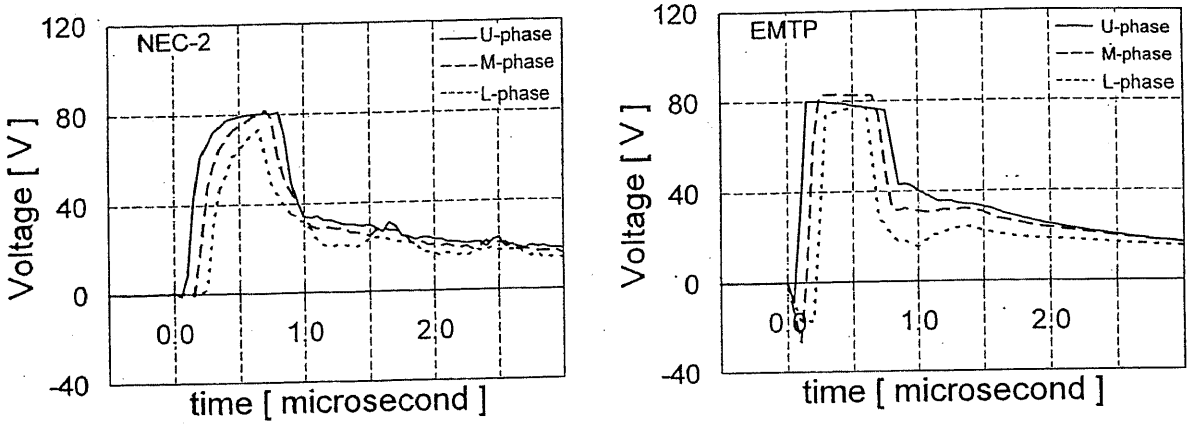

(a) Response for the step current injection.

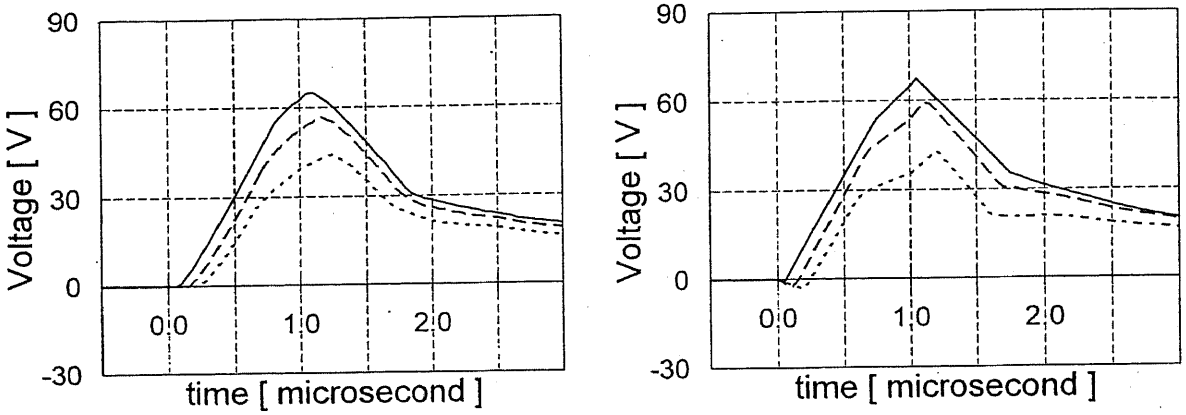

(b) Response for 1μs ramp current injection.

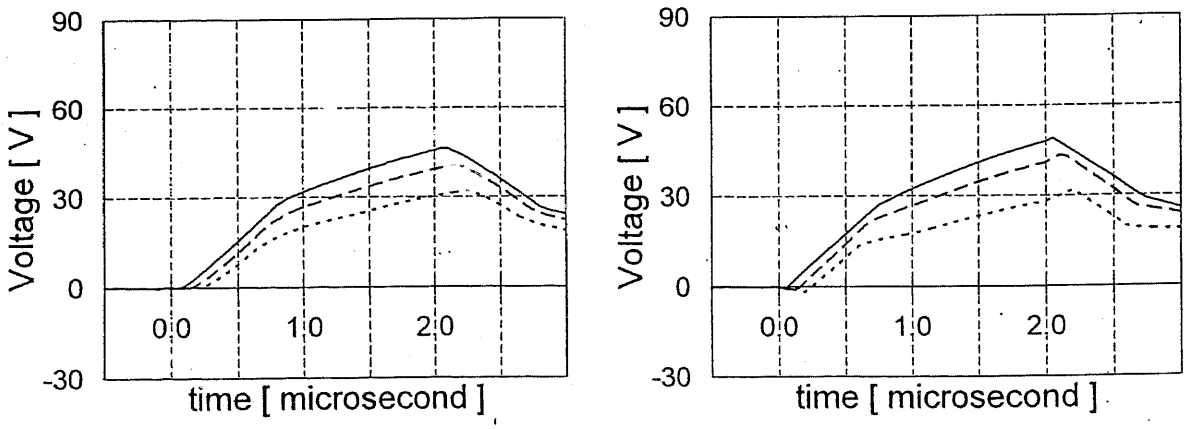

(c) Response for 2μs ramp current injection.

Fig. 5.11 Waveforms of insulator voltages of the model tower computed by EMTP or NEC-2.

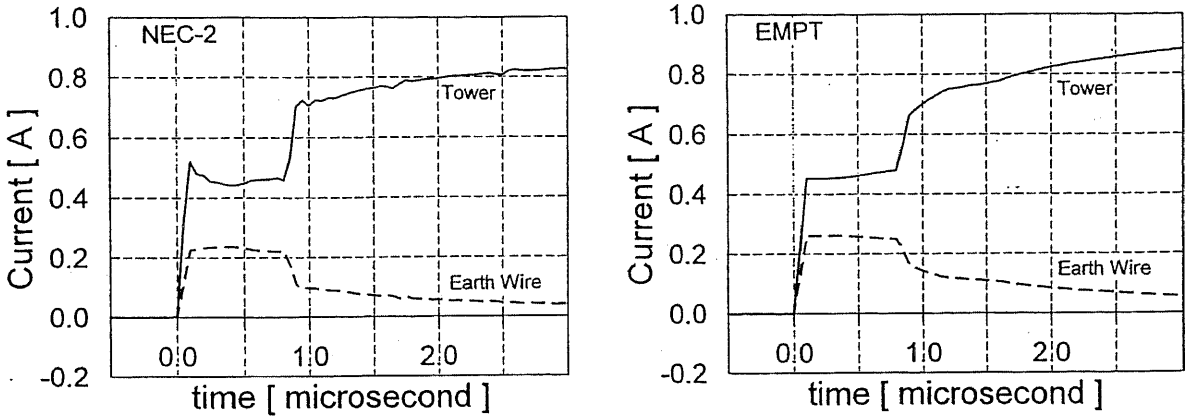

(a) Response for the step current injection.

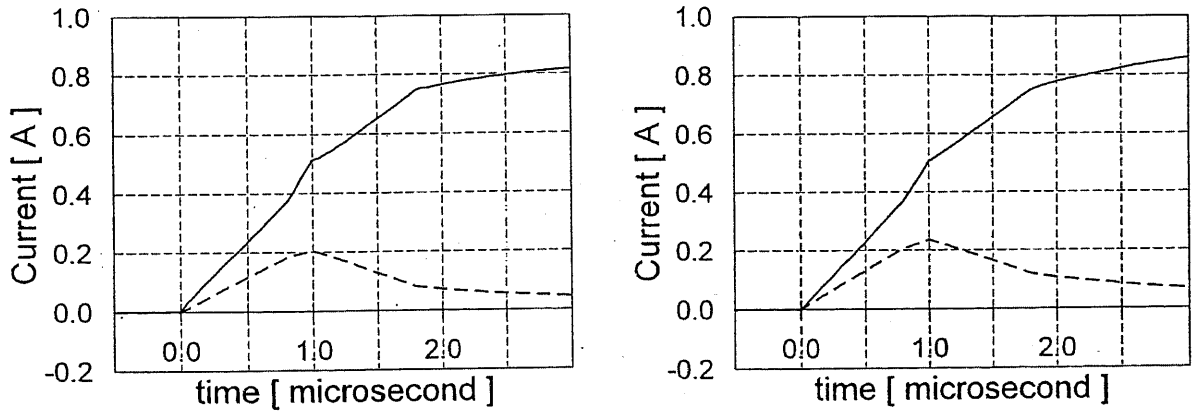

(b) Response for $1\mu s$ ramp current injection.

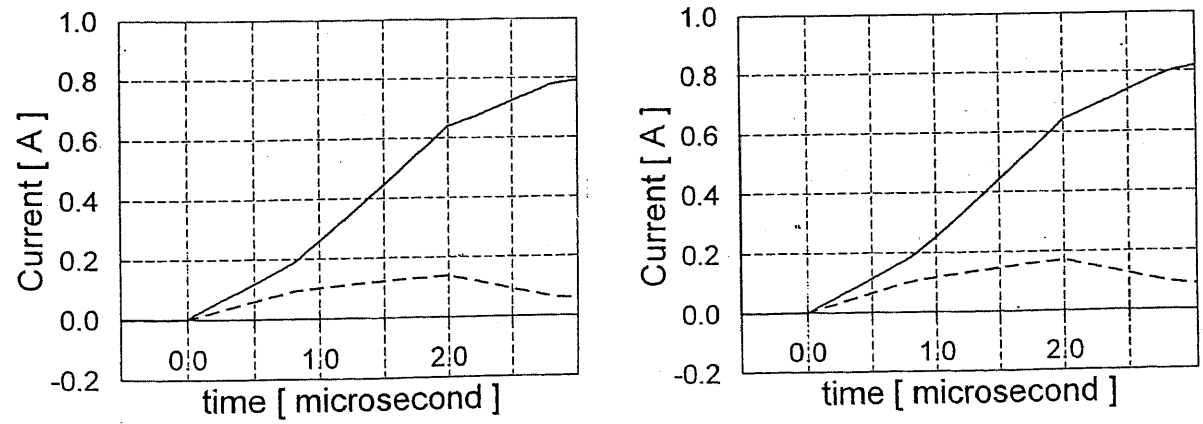

(c) Response for $2\mu s$ ramp current injection.

Fig. 5.12 Waveforms of the currents splitting into the tower and an earth wire computed by EMTP or NEC-2.

Chapter 6

Conclusions

The applicability of NEC-2 to the electromagnetic field analysis of tower surge response is verified by comparing the computed results with experimental results on simple structures. The difference is less than about 5 %, which is within the accuracy maintained in the measurements. Although there are some restrictions in the structures that can be properly modeled for NEC-2, it is much more flexible than the classical modeling of a tower by a cylinder or a cone.

On the basis of the analyses simulating various experimental methods by NEC-2, the surge impedance of an independent double-circuit tower is estimated to be about 150 Ω when it is evaluated by the direct method, where a current lead wire simulating a lightning channel is stretched vertically and a voltage measuring wire is stretched horizontally. The tower surge impedance representing the current splitting ratio at the tower top for a vertical stroke to the tower is higher than that characterized by the direct method for more than 25 %. On the other hand, the tower surge impedance representing the current splitting ratio for a stroke to mid-span or to an adjacent tower is about 10 % lower than that characterized by the direct method. The difference comes from different electromagnetic field around the tower influenced mainly by the electric fields associated with the fast-front currents propagating the tower, the earth wire and the current lead wire.

The surge characteristics of an earth-wired tower struck by a vertical lightning stroke are studied with the help of NEC-2. They are little influenced by the type of the lightning current, whether it is generated by a return stroke or it is generated by a downward traveling current wave.

The tower footing impedance evaluated from the reflected current exhibits initially a high value, which gradually falls off to the footing resistance. This apparent high footing impedance is physically ascribable to the distortion of the current wave propagating a tower. The distortion is partly caused by the strong axial electric field associated with the fast-front current wave itself, and is partly caused by the base-broadened structure peculiar to double-circuit towers, where a tower and its image behave as a non-homogeneous waveguide.

The coupling coefficient between the earth wire and a phase conductor is much lower than that in the TEM mode when it is evaluated at the moment of the peak of the insulator voltage even if a ramp current having a rise time of as long as 2μs is injected. This effect is due to the transient upward electric field generated by the vertical tower current, which cancels the downward field produced by the charge in the earth wire.

A procedure to determine the circuit parameters of the multistory tower model for the EMTP multi-conductor analysis, on the basis of the measured insulator voltages of an earth-wired tower, is proposed. The multistory model employing the proposed parameters can well reproduce the measured insulator voltages. The recommended surge impedance of the top of the multistory tower model is 200 Ω for a typical earth-wired double-circuit tower, which is about 35 % higher than that of the same tower without earth wires. This higher value takes account of the initially low coupling coefficients. The important fact to remember is that in determination of the circuit parameters, experimental results of an earth-wired tower should be used.

Parts of the above results have been incorporated into the latest technical report on evaluation methods of lightning surges on overhead power transmission lines and substations, prepared by an investigation committee of IEE Japan, and therefore they are expected to contribute to the improvement of the accuracy in lightning surge analysis.

Bibliography

[1] M. Ishii and J. Hojo : "Evaluation of lightning fault rate of EHV transmission line based on lightning parameters derived from electromagnetic field observation," *Trans. IEE Japan*, vol.111-B, no.5, pp.535-542, May 1991. (*in Japanese*)

[2] R. E. Orville and H. Songster : "The east coast lightning detection network," *IEEE Trans. Power Delivery*, vol.2, no.3, pp.899-907, July. 1987.

[3] Committee of Lightning Protection Design : "Lightning location systems in Japan and a lightning frequency map using the data obtained by them," *Trans. IEE Japan*, vol.116-B, no.4, pp.395-402, Apr. 1996. (*in Japanese*)

[4] Lightning Protection Design Study Committee : "Lightning proof design guide-book for transmission lines," CRIEPI Report, no.175031, Mar. 1976. (*in Japanese*)

[5] IEEE Working Group on Estimating Lightning Performance of Transmission lines : "IEEE guide for improving the lightning performance of transmission lines," IEEE Std 1243-1997, Dec. 1997.

[6] IEEE Modeling and Analysis of System Transients Working Group : "Modeling guidelines for fast front transients," *IEEE Trans. Power Delivery*, vol.11, no.1, pp.493-506, Jan. 1996.

[7] Investigation Committee for Advanced Evaluation Methods of Lightning Surges : "Modeling for advanced evaluation of lightning surges," Technical Report of IEE Japan, no.704, Nov. 1998. (*in Japanese*)

[8] M. Kawai : "Studies of the surge response on a transmission tower," *IEEE Trans. Power Apparatus and Systems*, vol.83, no.1, pp.30-34, Jan. 1964.

[9] M. Ishii, T. Kawamura, T. Kouno, E. Ohsaki, K. Shiokawa, K. Murotani and T. Higuchi : "Multistory transmission tower model for lightning surge analysis," *IEEE Trans. Power Delivery*, vol.6, no.3, pp.1327-1335, Jul. 1991.

[10] H. Matsubara and H. Motoyama : "The field test of lightning surge on the 500kV testing transmission tower," CRIEPI Report, no.T91093, 1992. (*in Japanese*)

[11] T. Yamada, A. Mochizuki, J. Sawada, E. Zaima, T. Kawamura, A. Ametani, M. Ishii and S. Kato : "Experimental evaluation of a UHV tower model for lightning surge analysis," *IEEE Trans. Power Delivery*, vol.10, no.1, pp.393-402, Jan. 1995.

[12] G. D. Breuer, A. J. Schultz, R. H. Schlomann and W. S. Price : "Field studies of the surge response of a 345-kv transmission tower and ground wire," *AIEE Trans. Power Apparatus and Systems*, vol.76, pp.1392-1396, Feb. 1958.

[13] R. W. Caswell, I. B. Johnson, E. F. Koncel and N. R. Shultz : "Lightning performance of 138-kv twin-circuit transmission lines of commonwealth Edison company — operating experience and field studies," *AIEE Trans. Power Apparatus and Systems*, vol.76, pp.1480-1491, Feb. 1958.

[14] F. A. Fisher, J. G. Anderson and J. H. Hagenguth : "Determination of lightning response of transmission lines by means of geometrical models," *AIEE Trans.* pt.III, vol.78, pp.1725-1736, Feb. 1960.

[15] M. A. A. Wahab, I. Matsubara and H. Kinoshita : "An experimental evaluation of some factors affecting tower surge impedance," *Trans. IEE Japan*, vol.107-E, no.9/10, pp.171-178, Sep./Oct. 1987.

[16] H. Motoyama : "Experimental study of lightning surge characteristics on transmission tower and transmission lines using a scale model," CRIEPI Report, no.T96074, Jun. 1997. (*in Japanese*)

[17] S. Hayashi, A. Kishima and H. Yamada : "Fundamental study of surge response of transmission line towers by means of scale models," *J. IEE Japan*, vol.87-1, no.940, pp.158-163, Jan. 1967. (*in Japanese*)

[18] W. A. Chisholm, Y. L. Chow and K. D. Srivastava : "Lightning surge response of transmission towers," *IEEE Trans. Power Apparatus and Systems*, vol.102, no.9, pp.3232-3242, Sep. 1983.

[19] C. F. Wagner and A. R. Hileman : "A new approach to to the calculation of the lightning performance of transmission lines III — a simplified method: stroke to tower," *AIEE Trans. Power Apparatus and Systems*, vol.79, pp.589-603, Oct. 1960.

[20] R. Lundholm, R. B. Finn and Jr, W. S. Price : "Calculation of transmission line lightning voltages by field concepts," *AIEE Trans. Power Apparatus and Systems*, vol.77, pp.1271-1283, Feb. 1958.

[21] K. Okumura and A Kishima : "A method for computing surge impedance of transmission tower by electromagnetic field theory," *Trans. IEE Japan*, vol.105-B, no.9, pp.733-740, Sep. 1985. (*in Japanese*)

[22] H. Takahashi : "New derivation method of the surge impedance on the tower model of a vertical conductor by the electromagnetic field theory," *Trans. IEE Japan*, vol.113-B, no.9, pp.1029-1036, Sep. 1993. (*in Japanese*)

[23] Y. Matsumoto, O. Sakuma, K. Shinjo, M. Saiki, T. Wakai, T. Sakai, H. Nagasaka, H. Motoyama and M. Ishii : "Measurement of lightning surges on test transmission line equipped with arresters struck by natural and triggered lightning," *IEEE Trans. Power Delivery*, vol.11, no.2, pp.996-1002, Apr. 1996.

[24] K. Shinjo, Y. Matsumoto, O. Sakuma, T. Wakai, T. Sakai, M. Ishii and H. Motoyama : "Characteristics of transient response of Okushishiku test transmission line struck by natural and triggered lightning," *Trans. IEE Japan*, vol.117-B, no.4, pp.478-487, Apr. 1997. (*in Japanese*)

[25] H. Motoyama, K. Shinjo, Y. Matsumoto and N. Itamoto : "Observation and analysis of multiphase back flashover on the Okushishiku test transmission line caused by winter lightning," *IEEE Trans. Power Delivery*, vol.13, no.4, pp.1391-1398, Oct. 1998.

[26] T. Shindo and T. Suzuki : "A new calculation method of breakdown voltage-time characteristics of long air gaps," *IEEE Trans. Power Apparatus and Systems*, vol.104, no.6, pp.1556-1563, Jun. 1985.

[27] H. Motoyama : "Experimental study and analysis of breakdown characteristics of long air gaps with short tail lightning impulse," *IEEE Trans. Power Delivery*, vol.11, no.2, pp.972-979, Apr. 1996.

[28] S. Kato and S. Okabe : "Study of loop voltage method in tower surge response analysis," *Trans. IEE Japan*, vol.115-B, no.5, pp.517-523, May 1995. (*in Japanese*)

[29] R.F.Harrington : "Field computation by moment methods," Macmillan Company, New York, 1968.

[30] E. K. Miller, L. Medgyesi-Mitschang and E. H. Newman : "Computational electromagnetics — frequency-domain method of moments," IEEE Press, ISBN 0-87942-276-9, 1992.

[31] K. S. Yee : "Numerical Solution of initial boundary value problems involving Maxwell's equations in isotropic media," *IEEE Trans. Antennas and Propagat.*, vol.14, no.4, pp.302-307, May 1996.

[32] L. Grcev and F. Dawalibi : "An electromagnetic model for transients in grounding systems," *IEEE Trans. Power Delivery*, vol.5, no.4, pp.1773-1781, Nov. 1990.

[33] S. Kato, R. Elarbi, A. Mochizuki and E. Zaima : "Surge response analysis of tower grounding by numerical electromagnetic field analysis," *Trans. IEE Japan*, vol.115-B, no.8, pp.970-977, Aug. 1995. (*in Japanese*)

[34] G. J. Burke and A. J. Poggio : "Numerical electromagnetic code (NEC) — method of moments," Naval Ocean Systems Center, Technical Document 116, San Diego, Jan. 1980.

[35] G. J. Burke : "Numerical electromagnetic code (NEC-4) — method of moments," Lawrence Livermore National Laboratory, UCRL-MA-109338 Pt. II, Jan. 1992.

[36] D. Adler : "Software exchange report," Applied Computational Electromagnetics Society Newsletter, vol.10, no.3, p.8, Nov. 1995.

[37] T. Hara, O. Yamamoto, M. Hayashi and C. Uenosono : "Empirical formulas of surge impedance for single and multiple vertical cylinder," *Trans. IEE Japan*, vol.110-B, no.2, pp.129-137, Feb. 1990. (*in Japanese*)

[38] T. Hara, W. Ouyang, O. Yamamoto, M. Hayashi, T. Nagai and O. Takeuchi : "Transmission tower model for surge analysis," Proc. of the 2nd Annual Conference of Power & Energy Society, IEE Japan, Session II, no.270, Fukuoka, Jul. 1991. (*in Japanese*)

[39] W. A. Chisholm, Y. L. Chow and K. D. Srivastava : "Travel time of transmission towers," *IEEE Trans. Power Apparatus and Systems*, vol.104, no.10, pp.2922-2928, Oct. 1985.

[40] M. Ishii : "Experimental study for insulation design of overhead transmission lines," Ph.D. thesis, The University of Tokyo, Dec. 1975. (*in Japanese*)

[41] Y. Watanabe, S. Kato, A. Mochizuki and E. Zaima : "Surge characteristics of a miniature transmission tower model simulated upward lightning current path," *Trans. IEE Japan*, vol.114-B, no.10, pp.1066-1072, Oct. 1994. (*in Japanese*)

[42] K. Shinjo, T. Wakai, T. Sakai, H. Sugimoto and M. Ishii : "Seasonal characteristics of lightning channel and its relationship to transmission line faults," *Trans. IEE Japan*, vol.116-B, no.3, pp.332-337, Mar. 1996. (*in Japanese*)

[43] A. Asakawa, K. Miyake, S. Yokoyama, T. Shindo, T. Yokota and T. Sakai : "Two types of lightning discharges to a high stack on the coast of the sea of Japan in winter," *IEEE Trans. Power Delivery*, vol.12, no.3, pp.1222-1231, Jul. 1997.

[44] W. A. Chisholm and W. Janischewskyj : "Lightning surge response of ground electrodes," *IEEE Trans. Power Delivery*, vol.4, no.2, pp.1329-1337, Apr. 1989.

[45] S. Kato, M. Takamatsu, K. Hidaka, S. Okabe and E. Zaima : "Conditions of the TEM approximation applicable to the surge analysis of transmission lines," National Convention Record of IEE Japan, no.1197, Chiba, Mar. 1992. (*in Japanese*)

[46] T. Hara and O. Yamamoto : "Modelling of a transmission tower for lightning surge analysis," IEE Proc. Gener. Transm. Distrb., vol.143, no.3, pp.283-289, May 1996.

[47] E. A. Oufi, A. S. AlFuhaid and M. M. Saied : "Transient analysis of lossless single-phase nonuniform transmission lines," *IEEE Trans. Power Delivery*, vol.9, no.3, pp.1694-1700, Jul. 1994.

[48] M. E. Almeida and M. T. Correia de Barros : "Tower modelling for lightning surge analysis using electro-magnetic transients program," IEE Proc. Gener. Transm. Distrb., vol.141, no.6, pp.637-639, Nov. 1994.

[49] M. T. Correia de Barros and M. E. Almeida : "Computation of electromagnetic transients on nonuniform transmission lines," *IEEE Trans. Power Delivery*, vol.11, no.2, pp.1082-1091, Apr. 1996.

[50] H. V. Nguyen, H. W. Dommel and J. R. Marti : "Modeling of single-phase nonuniform transmission lines in electromagnetic transient simulations," *IEEE Trans. Power Delivery*, vol.12, no.2, pp.916-921, Apr. 1997.

[51] H. W. Dommel : "Digital computer solution of electromagnetic transients in single- and multi-phase networks," *IEEE Trans. Power Apparatus and Systems*, vol.88, no.4, pp.388-398, Apr. 1969.

[52] N. Nagaoka : "A development of frequency-dependent tower model," *Trans. IEE Japan*, vol.111-B, no.1, pp.51-56, Jan. 1991. (*in Japanese*)

[53] S. Kato, A. Mochizuki and E. Zaima : "Transmission line models of tower in frequency domain," *Trans. IEE Japan*, vol.115-B, no.5, pp.524-531, May 1995. (*in Japanese*)

[54] "ATP user's rule book," K. U. Leuven EMTP Center , Jul. 1987.

[55] "RCS computer program BRACT, log-periodic scattering array program II," MBAssociates Report, no.MB-R-69/46, Contact no.F04801-68-C-0188, 1969.

[56] "Antenna modeling program," MBAssociates Report, no.MB-R-74/46, 74/62, 1974.

[57] "Antenna modeling program — supplementary computer program manual (AMP2)," MBAssociates Report, no.MB-R-75/4, 1975.

[58] G. J. Burke and E. K. Miller : "Modeling antennas near to and penetrating a lossy interface," *IEEE Trans. Antennas and Propagation*, vol.32, no.10, pp.1040-1049, Oct. 1984.

[59] H. Nakano : "Elementary course in antenna analysis by the method of moments," The 4th Workshop for Design and Analysis in Antennas and Propagations of IEICE Japan, Tokyo, Nov. 1994. (*in Japanese*)

[60] K. Sawaya : "Intermediate course in antenna analysis by the method of moments," The 12th Workshop for Design and Analysis in Antennas and Propagations of IEICE Japan, Kofu, Yamanashi, Sep. 1998. (*in Japanese*)

Papers Presented by the Author

TRANSACTIONS PAPERS

1. Y. Baba, M. Ishii and H. Kanatsuji : "Application of numerical electromagnetic code to analysis of tower surge response," *Trans. IEE Japan*, vol.116-B, no.7, pp.873-878, Jul. 1996. (*in Japanese* 馬場・石井・金辻：「数値電磁界解析手法による鉄塔インピーダンスの検討」, 電気学会論文誌B.)

2. M. Ishii and Y. Baba : "Surge impedance of independent transmission tower characterized by direct method," *Trans. IEE Japan*, vol.117-B, no.6, pp.845-850, Jun. 1997. (*in Japanese* 石井・馬場：「直接法で評価される鉄塔単体のインピーダンス」, 電気学会論文誌B.)

3. Y. Baba and M. Ishii : "Lightning surge characteristics of power transmission line studied by numerical electromagnetic code," *Trans. IEE Japan*, vol.118-B, no.9, pp.1028-1034, Sep. 1998. (*in Japanese* 馬場・石井：「数値電磁界解析手法による送電線サージ特性の検討」, 電気学会論文誌B.)

4. M. Ishii and Y. Baba : "Numerical electromagnetic field analysis of tower surge response," *IEEE Trans. Power Delivery*, vol.12, no.1, pp.483-488, Jan. 1997.

5. Y. Baba and M. Ishii : "Numerical electromagnetic field analysis on measuring methods of tower surge impedance," *IEEE Trans. Power Delivery.* (*in press*)

INTERNATIONAL CONFERENCES

6. M. Ishii and Y. Baba : "Numerical electromagnetic field analysis of tower surge response," *IEEE PES 1996 Summer Meeting*, 96 SM 436-6 PWRD, Denver, Colorado, Jul. 1996.

7. Y. Baba and M. Ishii : "Numerical electromagnetic field analysis on measuring methods of tower surge impedance," Proc. of Int. Conf. on Electrical Engineering (*ICEE 97*), F07, Matsue, Japan, Jul. 1997.

8. Y. Baba and M. Ishii : "Tower models for fast-front lightning currents," Proc. of Int. Workshop on High Voltage Engineering (*IWHV 99*), SP-99-14/HV-99-14, Okinawa, Japan, Jan. 1999.

9. Y. Baba and M. Ishii : "Application of numerical electromagnetic code to lightning surge analysis of overhead transmission lines," Proc. of Int. Symp. on Lightning Protection (*V SIPDA*), Sao Paulo, Brazil, Jun. 1999. (*accepted*)

DOMESTIC CONFERENCES

10. Y. Baba and M. Ishii : "Application of numerical electromagnetic code to analysis of tower surge characteristics," Joint Conference on Electrical Discharge and High Voltage Engieering of IEE Japan, ED-95-215/HV-95-86, Yokohama, Oct. 1995. (*in Japanese* 馬場・石井：「数値電磁界解析手法を用いた鉄塔サージ特性の検討」, 電気学会放電・高電圧合同研究会資料.)

11. Y. Baba and M. Ishii : "Analysis on measuring methods of tower surge impedance by using numerical electromagnetic code," Joint Conference on Electrical Discharge and High Voltage Engieering of IEE Japan, ED-96-203/HV-96-103, Nagoya, Nov. 1996. (*in Japanese* 馬場・石井：「数値電磁界解析手法による鉄塔インピーダンス測定法の検討」, 電気学会放電・高電圧合同研究会資料.)

12. Y. Baba and M. Ishii : "Traveling wave analysis of insulator voltage of transmission tower taking account of surge corona," Conference on High Voltage Engieering of IEE Japan, HV-97-80, Kyoto, Jul. 1997. (*in Japanese* 馬場・石井：「サージコロナを考慮した雷サージの進行波解析」, 電気学会高電圧研究会資料.)

13. Y. Baba and M. Ishii : "Study of lightning surge characteristics of transmission line by numerical electromagnetic code," Joint Conference on Electrical Discharge and High Voltage Engieering of IEE Japan, ED-97-118/HV-97-102, Toyama, Oct. 1997. (*in Japanese* 馬場・石井：「数値電磁界解析手法による送電線サージ特性の検討」, 電気学会放電・高電圧合同研究会資料.)

14. Y. Baba and A. Yokoyama : "Damping enhancement of low-frequency oscillation by adaptive neuro-controller of generator," National Convention Record of IEE Japan, no.1362, Sapporo, Mar. 1995. (*in Japanese* 馬場・横山：「適応型ニューロ発電機制御系による長周期動揺の抑制」, 平成７年電気学会全国大会.)

15. Y. Baba and M. Ishii : "Calculation of tower surge impedance using numerical electromagnetic field analysis," Proc. of the 6th Annual Conference of Power & Energy Society, IEE Japan, Session II, no.405, Nagoya, Aug. 1995.

16. Y. Baba and M. Ishii : "Influence of tower elements on tower surge response," National Convention Record of IEE Japan, no.1623, Tokyo, Mar. 1996. (*in Japanese* 馬場・石井：「鉄塔サージ特性への鉄塔構成要素の影響」, 平成８年電気学会全国大会.)

17. M. Ishii and Y. Baba : "Study of measuring methods of tower surge characteristics by numerical electromagnetic code," National Convention Record of IEE Japan, no.1624, Tokyo, Mar. 1996. (*in Japanese* 馬場・石井：「鉄塔サージ特性測定法の数値電磁界解析による検討」, 平成８年電気学会全国大会.)

18. Y. Baba and M. Ishii : "Surge impedance of isolated tower for lightning surge analysis," Proc. of the 7th Annual Conference of Power & Energy Society, IEE Japan, Session I-J, no.34, pp.197-201, Osaka, Aug. 1996. (*in Japanese* 馬場・石井：「雷サージ解析のための鉄塔単体のインピーダンスの検討」, 平成８年電気学会電力・エネルギー部門大会.)

19. Y. Baba and M. Ishii : "Influence of arrangement of auxiliary wires on measured tower surge impedance," Proc. of the 7th Annual Conference of Power & Energy Society, IEE Japan, Session II, no.428, Osaka, Aug. 1996. (*in Japanese* 馬場・石井：「鉄塔インピーダンス測定における補助線配置の影響」, 平成８年電気学会電力・エネルギー部門大会.)

20. Y. Baba and M. Ishii : "Tower surge impedance characterized by refraction method," National Convention Record of IEE Japan, no.1776, Kyoto, Mar. 1997. (*in Japanese* 馬場・石井：「透過波法で評価される鉄塔インピーダンス」, 平成９年電気学会全国大会.)

21. S. Sekioka, Y. Baba and M. Ishii : "Fundamental study on surge propagation characteristcs of substation bus," Record of Kansai-Branch Convention of IEE Japan, G5-2, Osaka, Nov. 1997. (*in Japanese* 関岡・馬場・石井：「気中絶縁電気所における母線サージ伝搬特性に関する基礎的検討」, 平成9年電気関係学会関西支部連合大会.)

22. Y. Baba and M. Ishii : "Difference in lightning surge characteristics of transmission tower stressed by direct hit or mid-span stroke," National Convention Record of IEE Japan, no.1644, Yokohama, Mar. 1998. (*in Japanese* 馬場・石井：「直撃雷と径間雷に対する送電線鉄塔の過渡応答特性の差」, 平成10年電気学会全国大会.)

23. Y. Baba and M. Ishii : "Circuit parameters for transmission tower for back-flashover analysis," Proc. of the 9th Annual Conference of Power & Energy Society, IEE Japan, Session II, no.362, Tokyo, Aug. 1998. (*in Japanese* 馬場・石井：「逆フラッシオーバ解析のための鉄塔パラメータに関する検討」, 平成10年電気学会電力・エネルギー部門大会.)

24. Y. Baba and M. Ishii : "Transient behavior of tower grounding impedance studied by numerical electromagnetic analysis," National Convention Record of IEE Japan, Yamaguchi, Mar. 1999. (*in Japanese* 馬場・石井：「数値電磁界解析手法による鉄塔接地インピーダンスの検討」, 平成11年電気学会全国大会.)

OTHER ORAL PRESENTATIONS

25. Y. Baba : "Application of antenna modeling program to lightning surge analysis," The 119th Conference on High Voltage Technology, no.119-14, Tokyo, Nov. 1997. (*in Japanese* 馬場：「アンテナ理論の雷サージ解析への応用」, 第119回高電圧技術研究会資料.)

26. Y. Baba and M. Ishii : "Application of antenna modeling program to analysis on lightning surge response of transmission tower," Proc. of the 3rd Seoul National University – The University of Tokyo Joint Seminar on Electrical Engineering, Tokyo, Jan. 1998.

27. M. Ishii and Y. Baba : "Modeling of towers under very fast-front lightning currents," IEEE Task Force Report, Jul. 1998.

THESES

- Y. Baba : "Damping enhancement of low-frequency oscillation by adaptive neuro-controller of generator," Graduation Thesis, The University of Tokyo, Feb. 1994. (*in Japanese* 馬場：「ニューラルネットワークの電力系統安定化制御への適用に関する研究」, 卒業論文.)

- Y. Baba : "Numerical electromagnetic field analysis of tower surge response," Master's Thesis, The University of Tokyo, Feb. 1996.

Acknowledgements

The author would like to express his deepest gratitude to Prof. Masaru ISHII for supervising and encouraging him to complete this thesis. He gave the author many opportunities to participate in the research conferences and meetings, in which the author was able to make friends with excellent young researchers, who inspired the author very much.

The author wishes to express his appreciation to Prof. Tadashi TAKANO of Institute of Space and Astronautical Science, Prof. Shohei KATO of Toyo University, Mr. Ichiro MATSUBARA of Osaka University, Dr. Hideki MOTOYAMA of Central Research Institute of Electric Power Industry, and Dr. Shozo SEKIOKA of Kansai Tech Corp., for their precious comments and fruitful discussions.

The author sincerely appreciates Mr. Wen-Wei LIAO of Yamabishi Electric Co. and Mr. Hiroaki KANATSUJI of Tokyo Electric Power Co., who are graduates of Prof. ISHII's High Voltage Laboratory. They kindly taught the author how to use the NEC-2 code.

The author is grateful to the Japan Society for the Promotion of Science for the financial support through the Special Research Fellowship Program.

Finally, the author would like to thank the old and new members of Prof. ISHII's Laboratory, Dr. Jun-Ichi HOJO, a research associate of this laboratory, Mr. Sei-Ichi SATO of Iwate Industrial and Technical Junior College, Mr. Kei NINOMIYA of Kitakyushu National College of Technology, Dr. Syarif HIDAYAT of Bandung Institute of Technology in Indonesia, Mr. Toshihisa KADOYA of Kansai Electric Power Co., Mr. Hirotoshi SAOTOME of Toshiba Corp., Mr. Kazuhiko SHIMIZU of East Japan Railway Co., Miss Sachiko OKADA of Hitachi, Ltd., Mr. Mikihisa SAITO, Mr. Tomoya MINAKAWA, Mr. Kou SATO, Mr. Ramesh K. POKHAREL, and Mr. Fumihiko TOKUDA for their cooperations and encouragements. Thanks to them, the author has been able to live a research life to the fullest for about five years.

December 18, 1998

Yoshihiro Baba

Appendix A

NEC-MoM Codes

A.1 History and Availability of NEC-MoM Codes

The first in a series of NEC-MoM codes was BRACT [55] developed at MBAssociates in San Ramon, California. BRACT solved Pocklington's integral equation for thin wires with a three-term sinusoidal current expansion and point matching of the boundary condition. This code could model wire antennas including the effect of interaction with a finitely conducting ground through the Fresnel reflection-coefficient approximation. However, BRACT was used mainly by its developers.

The Antenna Modeling Program (AMP) [56] was the first code released for use by public users. AMP also solved Pocklington's integral equation for thin wires with a three-term sinusoidal current expansion and point matching. The current expansion was chosen so that the current on a segment, with the form $A_i + B_i sin$ ks $+C_i cos$ ks, when extrapolated to the centers of the adjacent segments would coincide with the values of current on those segments. At a junction of several wires, the current was extrapolated to the center of a "phantom segment" whose length was the average of the connected segments. This extrapolation procedure smoothed the current distribution along wires, but still left discontinuities in current and charge density. AMP included options to model lumped or distributed loading on wires, transmission lines and networks.

AMP-2 [57] included a magnetic field integral equation model for surfaces while the previous version was restricted to modeling thin wires.

NEC-1 was developed from AMP-2. It included a new way of implementing the three-term sinusoidal current expansion so that current and charge density exactly satisfied continuity conditions imposed at the junctions. The current was forced to satisfy Kirchhoff's current law

at the junction, and the charge densities on wires were related to a function of the log of wire radius to provide approximate continuity of potential.

NEC-2 [34] added a solution for wires over a lossy ground by implementing the rigorous Sommerfeld-integral approach.

NEC-3 [58] extended the Sommerfeld-integral ground model to wires buried in the ground or penetrating from air into ground.

NEC-4 [35] retaines all of the capabilities of NEC-3, with changes and additions to improve the accuracy for stepped-radius wires and electrically small segments, and to add end caps and insulated wires.

The author employs NEC-2 in the present study, since later versions, NEC-3 and NEC-4, are available only to the citizens of the United States and Canada, or to the users who are licensed from Lawrence Livermore National Laboratory [36].

The documentation for NEC-2 is officially available from the National Technical Information Service, U.S. Department of Commerce.

```
National Technical Information Service
U.S. Department of Commerce
Springfield, Virginia 22161
Phone :  + 1 - 703 - 487 - 4650
```

It consists of three volumes; the theory, the source code in Fortran and the user's guide. The current price is about 200 dollars.

The volumes of the theory and the user's guide are also obtained on a WWW site at

```
http://members.home.net/nec2/
```

The information on the free executables of NEC-2 and commercial programs sold by vendors are also available on the above site.

Recent materials on the MoM theory and its applications [59][60] contain detailed descriptions of the MoM, and they are useful for persons who wish to learn to use NEC-MoM codes.

A.2 Sample Input Data to NEC-2

Table A.1 Input data for the analysis in chapter 2 (single conductor).

```
CM    SINGLE VERTICAL CONDUCTOR OF CH. 2
CM         N=512 DT=1. 25E-09SEC
CE      PERFECTLY CONDUCTING GROUND
GW  1   10        0. 0        0. 0        3. 0        0. 0        0. 0        0. 0     0. 0025
GW  2   30        0. 0        9. 0        3. 0        0. 0        0. 0        3. 0     0. 0025
GW  3   10        0. 0        9. 0        3. 0        0. 0        9. 0        0. 0     0. 0025
GW  4   30        0. 0        0. 0        3. 0        9. 0        0. 0        3. 0     0. 0025
GW  5   10        9. 0        0. 0        3. 0        9. 0        0. 0        0. 0     0. 0025
GE  1
GN  1
LD  4    2   20   20   5. 0E+03
LD  4    3   10   10     467. 0
LD  4    5   10   10     467. 0
LD  4    4    1    1   1. 0E+04
FR  0  257    0    0    1. 5625    1. 5625
EX  0    2   20   00   5. 0E+03       0. 0
PT  0    4    1
XQ
EN
```

Table A.2 Input data for the analysis in chapter 2 (four parallel conductors).

```
CM    FOUR VERTICAL CONDUCTORS OF CH. 2
CM         N=512 DT=1. 25E-09SEC
CE      PERFECTLY CONDUCTING GROUND
GW  1   10        0. 0        0. 0        3. 0        0. 0        0. 0        0. 0     0. 0165
GW  2   10        0. 0      0. 404        3. 0        0. 0      0. 404        0. 0     0. 0165
GW  3   10      0. 404      0. 404        3. 0      0. 404      0. 404        0. 0     0. 0165
GW  4   10      0. 404        0. 0        3. 0      0. 404        0. 0        0. 0     0. 0165
GW  5    2        0. 0        0. 0        3. 0        0. 0      0. 404        3. 0     0. 0165
GW  6    2        0. 0      0. 404        3. 0      0. 404      0. 404        3. 0     0. 0165
GW  7    2      0. 404      0. 404        3. 0      0. 404        0. 0        3. 0     0. 0165
GW  8    2      0. 404        0. 0        3. 0        0. 0        0. 0        3. 0     0. 0165
GW  9   30      0. 202      9. 404        3. 0      0. 202      0. 404        3. 0     0. 0165
GW 10   10      0. 202      9. 404        3. 0      0. 202      9. 404        0. 0     0. 0165
GW 11   30      0. 404        0. 0        3. 0      9. 404        0. 0        3. 0     0. 0165
GW 12   10      9. 404        0. 0        3. 0      9. 404        0. 0        0. 0     0. 0165
GE  1
GN  1
LD  4    9   20   20   5. 0E+03
LD  4   10   10   10     467. 0
LD  4   12   10   10     467. 0
LD  4   11    1    1   1. 0E+04
FR  0  257    0    0    1. 5625    1. 5625
EX  0    9   20   00   5. 0E+03       0. 0
PT  0   11    1
XQ
EN
```

Table A.3 Input data for the analysis in chapter 4.

```
CM      BASE-BROADENED MODEL TOWER OF CH. 4
CM            INSULATOR VOLTAGE
CM          N=512 DT=5.0E-08SEC
CE       PERFECTLY CONDUCTING GROUND
GW  1    1      -5.0     -5.0    120.0    -5.0     -5.0    108.0     0.1
GW  2    1       5.0     -5.0    120.0     5.0     -5.0    108.0     0.1
GW  3    1       5.0      5.0    120.0     5.0      5.0    108.0     0.1
GW  4    1      -5.0      5.0    120.0    -5.0      5.0    108.0     0.1
GW  5    2      -5.0     -5.0    108.0    -5.0     -5.0     84.0     0.15
GW  6    2       5.0     -5.0    108.0     5.0     -5.0     84.0     0.15
GW  7    2       5.0      5.0    108.0     5.0      5.0     84.0     0.15
GW  8    2      -5.0      5.0    108.0    -5.0      5.0     84.0     0.15
GW  9    1      -5.0     -5.0     84.0    -5.0     -5.0     72.0     0.2
GW 10    1       5.0     -5.0     84.0     5.0     -5.0     72.0     0.2
GW 11    1       5.0      5.0     84.0     5.0      5.0     72.0     0.2
GW 12    1      -5.0      5.0     84.0    -5.0      5.0     72.0     0.2
GW 13    1      -5.0     -5.0     72.0    -5.0     -5.0     60.0     0.25
GW 14    1       5.0     -5.0     72.0     5.0     -5.0     60.0     0.25
GW 15    1       5.0      5.0     72.0     5.0      5.0     60.0     0.25
GW 16    1      -5.0      5.0     72.0    -5.0      5.0     60.0     0.25
GW 17    1      -5.0     -5.0     60.0    -6.2     -6.2     48.0     0.25
GW 18    1       5.0     -5.0     60.0     6.2     -6.2     48.0     0.25
GW 19    1       5.0      5.0     60.0     6.2      6.2     48.0     0.25
GW 20    1      -5.0      5.0     60.0    -6.2      6.2     48.0     0.25
GW 21    2      -6.2     -6.2     48.0    -8.6     -8.6     24.0     0.3
GW 22    2       6.2     -6.2     48.0     8.6     -8.6     24.0     0.3
GW 23    2       6.2      6.2     48.0     8.6      8.6     24.0     0.3
GW 24    2      -6.2      6.2     48.0    -8.6      8.6     24.0     0.3
GW 25    2      -8.6     -8.6     24.0   -11.0    -11.0      0.0     0.35
GW 26    2       8.6     -8.6     24.0    11.0    -11.0      0.0     0.35
GW 27    2       8.6      8.6     24.0    11.0     11.0      0.0     0.35
GW 28    2      -8.6      8.6     24.0   -11.0     11.0      0.0     0.35
GW 29    1      -5.0     -5.0    120.0     5.0     -5.0    120.0     0.1
GW 30    1       5.0     -5.0    120.0     5.0      5.0    120.0     0.1
GW 31    1       5.0      5.0    120.0    -5.0      5.0    120.0     0.1
GW 32    1      -5.0      5.0    120.0    -5.0     -5.0    120.0     0.1
GW 33   40       5.0     -5.0    600.0     5.0     -5.0    120.0     0.1
GW 34   40     -15.0     -5.0    108.0   -15.0   -485.0    108.0     0.1
GW 35    9     -15.0   -485.0    108.0   -15.0   -485.0      0.0     0.1
GW 36   40     -15.0     -5.0    108.0   -15.0    475.0    108.0     0.1
GW 37    9     -15.0    475.0    108.0   -15.0    475.0      0.0     0.1
GW 38    1      -5.0     -5.0    108.0   -15.0     -5.0    108.0     0.1
GW 39   40      -5.0     -5.0    120.0    -5.0   -485.0    120.0     0.1
GW 40   10      -5.0   -485.0    120.0    -5.0   -485.0      0.0     0.1
GW 41   40      -5.0      5.0    120.0    -5.0    485.0    120.0     0.1
GW 42   10      -5.0    485.0    120.0    -5.0    485.0      0.0     0.1
GE  1
GN  1
LD  4   33   40   40   5.0E+03
LD  4   35    9    9     461.0
LD  4   37    9    9     461.0
LD  4   40   10   10     467.0
LD  4   42   10   10     467.0
LD  4   38    1    1   1.0E+05
LD  4   25    2    2      40.0
LD  4   26    2    2      40.0
LD  4   27    2    2      40.0
LD  4   28    2    2      40.0
FR  0  257    0    0 3.906E-02 3.906E-02
EX  0   33   40   00   5.0E+03       0.0
PT  0   38    1
XQ
EN
```